

**LOW FREQUENCY SHEAR ALFVEN WAVE  
PROPAGATION AND ITS INTERACTION WITH  
CHARGED PARTICLES IN THE MAGNETOSPHERE**

*A Project Report*

*Submitted by*

**NITHIN SIVADAS  
AE08B014**

*in partial fulfilment of the requirements*

*for the award of the degree of*

**BACHELOR OF TECHNOLOGY *in*  
AEROSPACE ENGINEERING**

**&**

**MASTER OF TECHNOLOGY *in*  
AEROSPACE ENGINEERING**



**DEPARTMENT OF AEROSPACE ENGINEERING  
INDIAN INSTITUTE OF TECHNOLOGY MADRAS**

**JUNE 2013**

## **CERTIFICATE**

This is to certify that the report titled **LOW FREQUENCY SHEAR ALFVEN WAVE PROPAGATION AND ITS INTERACTION WITH CHARGED PARTICLES IN THE MAGNETOSPHERE**, submitted by **NITHIN SIVADAS (AE08B014)**, to the Indian Institute of Technology Madras, Chennai for the award of the degree of **Bachelor of Technology and Master of Technology**, is a bonafide record of the research work done by him under our supervision. The contents of this report, in full or in parts, have not been submitted to any other Institute or University for the award of any degree or diploma.

**Dr. T. M. Muruganandam**

Project Guide

Assistant Professor

Dept. of Aerospace Engineering

IIT-Madras, 600 036

**Prof. Harishankar Ramachandran**

Co-Guide

Professor

Dept. of Electrical Engineering

IIT-Madras, 600 036

Place: Chennai

Date: 14<sup>th</sup> June 2013

## ACKNOWLEDGEMENTS

Firstly, I wish to acknowledge my parents for introducing me to this curious world of science and engineering and endowing me with the freedom to pursue my passion.

Secondly, I acknowledge my two guides Prof. Harishankar Ramachandran and Dr. T. M. Muruganandam for the motivation and support that they gave me to pursue the project work of my interest. In particular, I have learnt a lot more than when I started the project, due to the continued interaction that I had with Prof. Harishankar Ramachandran and his willingness to spend a lot of his time in educating me on the fundamentals of plasma physics and electromagnetism.

Thirdly, I wish to thank Dr. Ananth Krishnan (Dept. of Electrical Engineering) and Dr. Ranjit Kumar Nada (Dept. of Physics) for the courses that they offered in Computational Electromagnetism and Computational Physics respectively. I am also very grateful to Mr. Praveen Venkatesh (3<sup>rd</sup> Year Electrical Engineering Student) for his time spent with me on developing the initial frameworks of the simulations.

I also wish to express my sincere gratitude to the IIT Madras Student Satellite team, who have closely interacted with me and discussed the intricacies of the presented work. I also thank Dr. Ranjith Mohan (Dept. of Aerospace Engineering) for the discussions we had on some of the fundamental concepts in Mathematics and Physics used in this work.

Lastly, I am grateful to Dr. P. Sreekumar and Dr. Manju Sudhakar from Space Astronomy Group, ISRO Satellite Centre, Bangalore, for their constant encouragement and support from my undergraduate years to pursue my interest in space physics.

## ABSTRACT

The Earth's magnetic field supports cold and hot plasma at altitudes higher than 1000 km, in the region called the magnetosphere. The hot plasma constitutes the Van Allen Radiation belt, composed of mainly high energy protons and electrons and interpenetrating the cold plasma. The plasma, especially near the Earth, are effectively trapped within the Earth's dipole magnetic field.

However, these highly energetic charged particles are sometimes precipitated to lower altitudes due to electromagnetic fluctuations in the static geomagnetic field. These particles can cause damages to satellites and health hazards for astronauts in Low Earth Orbits (LEO) altitudes, 500 to 1000 km. They are also thought to be the cause of the magnificent aurora borealis in the Arctic and Antarctic regions.

This study aims at understanding the nature and statistics of the precipitated high energy particles caused due to electromagnetic noise in the Van Allen radiation belts. In this report, a test particle analysis of the scattering of high energy particles by shear Alfvén noise in the Van Allen radiation belts is presented. Though there are several wave modes supported by the magnetosphere, the shear Alfvén wave mode was chosen for this study as they travel along the magnetic field line and remain confined within a narrow region.

The Alfvén wave noise was generated by carrying out a Finite Difference Time Domain (FDTD) simulation in Orthogonal Dipole Coordinate system with realistic plasma parameters and perfectly reflecting ionosphere boundary conditions. The shear Alfvén wave was modelled using the Linearized Magneto-hydrodynamic (MHD) theory, and it is valid only for frequencies lesser than Ion Cyclotron frequencies.

The simulation results showed a considerable scattering of the equatorial pitch angle of particles. The results closely matched the theoretical estimates derived from simple physical arguments. From the equatorial pitch angle distribution, the statistics of the precipitated particles were obtained in terms of the scattering of mirror point altitudes of the particles.

# TABLE OF CONTENTS

	<b>Page</b>
<b>ACKNOWLEDGEMENTS .....</b>	<b>i</b>
<b>ABSTRACT.....</b>	<b>ii</b>
<b>TABLE OF CONTENTS.....</b>	<b>iii</b>
<b>LIST OF FIGURES .....</b>	<b>vi</b>
<b>ABBREVIATIONS .....</b>	<b>viii</b>
<b>NOTATIONS .....</b>	<b>ix</b>
<b>1. INTRODUCTION.....</b>	<b>1</b>
1.1. Background.....	1
1.1.1. The Earth’s Inner Magnetosphere.....	1
1.1.2. The Van-Allen Radiation Belts .....	2
1.1.3. Wave-particle Interactions .....	3
1.2. Review of Previous Work .....	3
1.3. Outline of the Report .....	4
1.4. Applications of the Present Work .....	4
<b>2. BASIC PHYSICS INVOLVED .....</b>	<b>8</b>
2.1. Low-Frequency Alfvén Wave Propagation through Magnetized Plasma .....	8
2.2. Motion of Trapped Energetic Charged Particles in the Radiation Belt.....	10
2.2.1. Magnetic Dipole.....	10
2.2.2. The Three Kinds of Motion .....	11
2.2.3. Loss cone angle.....	13
2.3. Interaction of wave with particles in the radiation belts .....	13
<b>3. DESCRIPTION OF SIMULATIONS .....</b>	<b>15</b>
3.1. 3-D FDTD Simulation in Orthogonal Dipole Coordinates .....	15
3.1.1. Orthogonal Dipole Coordinate System .....	15
3.1.2. Simplified Maxwell’s equation for Electromagnetic waves .....	17

3.1.3.	Discretization of the Maxwell's equation .....	18
3.1.4.	Linearized MHD Equations .....	22
3.2.	Acquiring Realistic Plasma Parameters .....	23
3.2.1.	Magnetic Field Intensity .....	23
3.2.2.	Plasma Density.....	23
3.2.3.	Alfven Wave Velocity .....	23
3.3.	Generate Shear Alfven Wave Noise .....	27
3.3.1.	Sinusoidal Shear-Alfven Wave .....	27
3.3.2.	Dispersion Diagram of a Shear-Alfven Wave in the Plasmasphere .....	28
3.3.3.	Randomizing the Phase-spectrum of the Shear-Alfven Wave .....	30
3.4.	3-D Trajectory Solver for Charged Particles in the Radiation Belts .....	32
3.5.	Incorporation of 3-D Alfven Wave noise into the 3-D Trajectory Solver .....	34
3.6.	Acquiring the Equatorial Pitch Angle Distribution.....	34
<b>4.</b>	<b>RESULTS.....</b>	<b>35</b>
4.1.	Input Parameters .....	35
4.2.	Scattering of Equatorial Pitch Angle Distribution .....	35
4.3.	Scattering of Mirror Points .....	37
<b>5.</b>	<b>CONCLUSION .....</b>	<b>40</b>
5.1.	Summary .....	40
5.2.	Future Work .....	40
	<b>REFERENCES.....</b>	<b>41</b>
	<b>APPENDIX 1: Simulation Codes .....</b>	<b>43</b>
6.1.	3-D FDTD Simulations in Orthogonal Dipole Coordinate System .....	43
6.1.1.	main.m .....	44
6.1.2.	calculate.m .....	52
6.1.3.	calculateh1.m .....	52
6.1.4.	plot_mer.m .....	53
6.1.5.	plot_equ.m .....	53
6.1.6.	plot_fft_a.m.....	54

6.2.	Extracting plasma density from GCPM Ver 2.4.....	55
6.2.1.	Input file: input.txt .....	55
6.2.2.	main1.for.....	55
6.3.	3-D Particle Trajectory Solver .....	58
6.3.1.	lineartrap.m .....	59
6.3.2.	solve1.m.....	61
6.3.3.	cart2dip.m .....	62
6.3.4.	equatorial_pitch.m .....	62
6.3.5.	velocity.m.....	63
6.3.6.	Bfield_1.m .....	63
<b>APPENDIX II: Conference Poster .....</b>		<b>64</b>

## LIST OF FIGURES

Figure 1.1: Earth’s Magnetosphere being compressed by the solar wind and organized into a close cavity. (Illustrated by Eric A. Lord [10] ).....	5
Figure 1.2: A cross section of the inner magnetosphere with dipole field lines, plasmaphere, plasmopause and the typical energetic charged particle trajectory along the field line. [11] .....	6
Figure 1.3: Schematic cross-section of the Van Allen Radiation Belts that surround the Earth. The inner belt is mainly composed of energetic protons, while the outer belt is mainly energetic electrons. (R. A. Mewaldt, A.C. Cummings and E.C. Stone, EOS, 1994) [10].....	7
Figure 1.4: Typical trajectory of an energetic charged particle trapped within the geo-magnetic field. [12].....	7
Figure 2.1: Trajectory of two protons of 15 MeV in the Earth’s dipole magnetic field, generated by the 3-D Trajectory Solver described in Section 3.4 developed by the author. Isometric (above) and Top view (below) of the particle trajectories.....	12
Figure 2.2: The variation of loss cone angle (equatorial pitch angle below which the particle is lost due to collision with the Earth’s atmosphere) with respect to the McIlwain L coordinate, calculated using Eq. 2.14. ....	14
Figure 3.1: Flow chart of steps followed to attain the result.....	15
Figure.3.2: Plane $\mu=0$ . Top view of the plasmasphere. Blue circle in the centre represents the Earth.....	20
Figure 3.3: Plane $\phi=0$ . Cross sectional view of the plasmasphere. Blue semi-circle towards the left-side of the figure represents one-half of the Earth.....	20
Figure 3.4: Plane $\mu = 0$ . EM source with $E_\phi$ polarization, and $\partial\partial\phi = 0$ .....	21
Figure 3.5: Plane $\phi=0$ . EM source with $E_\phi$ polarization. EM wave originating from a line source in $\mu = 0$ plane with $\partial/\partial\phi = 0$ , propagating in Vacuum and spreading isotropically outward in $\phi = 0$ plane as expected. ....	21
Figure 3.6: Plane $\mu = 0$ . Magnetic field intensity ( $B_0$ ) in log scale. ....	24
Figure 3.7: Plane $\phi=0$ . Magnetic field intensity ( $B_0$ ) in log scale.....	24
Figure 3.8: Plane $\mu=0$ . Electron (plasma) density ( $\rho$ ) in log scale. ....	25
Figure 3.9: Plane $\phi=0$ . Electron (plasma) density ( $\rho$ ) in log scale. ....	25
Figure 3.10: Plane $\mu=0$ . Alfven wave velocity ( $v_A$ ) in log scale.....	26
Figure 3.11: Plane $\phi=0$ . Alfven wave velocity ( $v_A$ ) in log scale.....	26
Figure 3.12: Shear-Alfven-wave mode with sinusoidal source polarized in $B_\phi$ ( $B_\phi$ is $\perp$ to the magnetic field line and k vector of the wave).....	27

Figure 3.13: Dispersion diagram of a Shear-Alfven Wave propagating in L=1.43....	29
Figure 3.14: Alfven Wave Velocity in m/s along L=1.43 .....	30
Figure 3.15: Amplitude Spectrum of the $B_\phi$ field of an Alfven Wave along L=1.4286.....	31
Figure 3.16: Phase Spectrum of the $B_\phi$ field of an Alfven Wave along L=1.4286. ...	31
Figure 3.17: Randomized Phase Spectrum of the $B_\phi$ field generated by random number generator. ....	31
Figure 3.18: $B_\phi$ (t=0.94 ms) noise of 6000 Hz bandwidth along space.....	32
Figure 3.19: The trajectory and the gyrocentre path of a 15 MeV proton in L-shell = 4 generated by the simulation module. ....	33
Figure 4.1: Initial (above) and scattered (below) equatorial pitch angle distribution (Total number of protons = 1000) .....	36
Figure 4.2: Gaussian fit on the scattered equatorial pitch angle distribution.....	37
Figure 4.3: Scattering of mirror point altitudes of the particles. ....	38
Figure 4.4: Variation of mirror point altitude with equatorial pitch angle.....	38

## ABBREVIATIONS

3D	Three Dimension(al)
DFFT	Discrete Fast Fourier Transform
ECT	Energetic Particle, Composition and Thermal Plasma Suite
EFW	Electric Field and Waves Suite
EM	Electromagnetic
EMFISIS	Electric and Magnetic Field Instrument Suite and Integrated Science
FDTD	Finite Difference Time Domain
FFT	Fast Fourier Transform
FWHM	Full Width at Half Maximum
GCPM	Global Core Plasma Model
IGRF	International Geomagnetic Reference Field
LEO	Low Earth Orbit
MHD	Magneto-Hydrodynamic
NASA	National Aeronautics and Space Administration
ODE	Ordinary Differential Equation
PML	Perfectly Matched Layer
RPS	Relativistic Proton Spectrometer

## NOTATIONS

		<b>Unit</b>
$\omega$	Wave frequency	[rad s <sup>-1</sup> ]
$\omega_{ci}$	Ion cyclotron frequency	[rad s <sup>-1</sup> ]
$v_A$	Alfven wave velocity	[m s <sup>-1</sup> ]
$\rho$	Plasma density	[kg m <sup>-3</sup> ]
$L$	McIlwain L Parameter	[ ]
$B_0$	Magnetic Field Intensity	[T]
$\mu_0$	Permeability of free space	[N A <sup>-2</sup> ]
$\mathbf{E}_1$	Electric field vector of the wave linearized to first order	[V m <sup>-1</sup> ]
$\mathbf{B}_1$	Magnetic field vector of the wave linearized to first order	[T]
$m_\sigma$	Mass of species $\sigma$	[kg]
$q_\sigma$	Charge of species $\sigma$	[C]
$\mathbf{E}_\perp$	Electric field perpendicular to the local magnetic field	[V m <sup>-1</sup> ]
$\mathbf{J}_\perp$	Current density perpendicular to the local magnetic field	[A m <sup>-2</sup> ]
$\mathbf{B}_{\mu 1}$	Linearized magnetic field parallel to the magnetic field line	[T]
$\mathbf{E}$	Total electric field vector	[V m <sup>-1</sup> ]
$\mathbf{B}$	Total magnetic field vector	[T]
$\gamma$	Relativistic factor	[ ]
$\mathbf{v}$	Velocity of the charged particle	[m s <sup>-1</sup> ]
$c$	Speed of light	[m s <sup>-1</sup> ]
$\Omega$	Cyclotron frequency	[rad s <sup>-1</sup> ]
$\rho_\Omega$	Cyclotron radius	[m]
$\mathbf{B}_{dip}$	Magnetic dipole field	[T]
$\mathbf{M}$	Magnetic moment vector	[A m <sup>2</sup> ]
$R_E$	Mean earth radii	[m]
$\tau_b$	Time period of bounce motion	[ s ]
$\tau_d$	Time period of drift motion	[ s ]
$\alpha_{eq}$	Equatorial pitch angle	[deg. ]
$\theta_m$	Elevation angle of the mirror point	[rad]
$\alpha_l$	Loss cone angle	[deg.]
$B_w$	Maximum magnetic field produced due to an EM wave	[T]
$V_\parallel$	Particle velocity parallel to the local geomagnetic field	[m s <sup>-1</sup> ]
$V_\perp$	Particle velocity perpendicular to the local geomagnetic field	[m s <sup>-1</sup> ]
$B_\phi^{noise}$	Magnetic field intensity of shear-Alfven wave noise	[T]
$E_v^{noise}$	Electric field intensity of shear-Alfven wave noise	[V m <sup>-1</sup> ]
$\Delta\alpha^{eq}$	Spread in the equatorial pitch angle distribution	[deg.]
$r_m$	Mirror point altitude (distance from the Earth's surface)	[km]

# CHAPTER 1

## 1. INTRODUCTION

The subject of the present work deals with the propagation of low-frequency shear Alfvén waves and its interaction with the trapped charged particles in the Earth's inner magnetosphere. This section is a brief introduction containing the background, outline and applications of the presented work.

### 1.1. Background

Above an altitude of about 1000 km, the Earth is surrounded by the Van-Allen Radiation belts that contain highly energetic charged particles (mainly protons and electrons) that are trapped within the geo-magnetic field. These highly energetic particles, are sometimes precipitated to lower altitudes, and can cause damages to satellites and health hazards for astronauts in Low Earth Orbits (500 to 1000 km). These Energetic plasma particles which can affect our technology, are also thought to be contributors of the aurora borealis in the northern and southern polar regions. The precipitation of these particles are caused mainly due to electro-magnetic fluctuations within the Van-Allen Radiation belts, and hence it is important to understand how these fluctuations affect the trajectories of these charged particles.

#### 1.1.1. The Earth's Inner Magnetosphere

The Earth's immediate environment consists of

1. The neutral atmosphere (up to 60 km above the Earth's surface)
2. The ionosphere, a region of highly ionized gas (heavy ions, protons and electrons) as well as neutral particles (extending up to 1000 km)
3. The magnetosphere consisting mainly of protons and electrons (extending up to 100,000 km)

There is an abrupt density increase in charged particles (cold plasma) as we move from the neutral atmosphere-ionosphere boundary (at approximately 300 km). However, there is no such sharp boundary between the ionosphere and the magnetosphere. In the magnetosphere, the behaviour of the plasma is controlled by the geomagnetic field. The solar wind exerts pressure on the magnetosphere, compressing it on the sun side (creating a boundary around  $10 R_E$  known as the magnetopause) and extending it into a long tail on the night side. Figure 1.1 depicts the entire magnetosphere.

However, the geo-magnetic field in the Inner Magnetosphere (extending from  $2 R_E$  up to  $7 R_E$ ), can be approximated to a dipole inclined with respect to the Earth's axis of rotation by about  $11^\circ$ . Features of the inner-magnetosphere are sketched in Figure 1.2. The plasma near the Earth, within the inner-magnetosphere, is 'frozen in' to the geomagnetic field. This region that extends to about  $4 R_E$  is called the plasmasphere. The plasmasphere is in approximate equilibrium with the ionosphere. The boundary of the plasmasphere, called the plasmapause, separates the magnetospheric plasma from the plasma co-rotating with the Earth in the plasmaphere.

The bulk of the plasma within the plasmasphere is composed mainly of cold electrons and protons with energies of a few electron volts, and is relatively dense with concentrations of  $10^2$  to  $10^4$  particles/cm<sup>3</sup>. This inner-magnetosphere region that hosts the Inner Van-Allen Radiation belts is the region of interest in the present work.

### **1.1.2. The Van-Allen Radiation Belts**

Interpenetrating the cold plasma of the plasmasphere, the inner-magnetosphere is also populated with energetic population of charged particles (hot plasma), which constitute the Van-Allen Radiation belts. This hot plasma contains electrons and protons of energy  $> 10$  keV to 100 MeV, that are magnetically trapped within the geo-magnetic field.

The source and loss processes of these energetic particles are not completely understood [1], but one possibility is that the particles of the solar wind enter the magnetosphere through the tail, and are accelerated along the magnetic field lines and enter the plasmasphere. An important loss process for the radiation belt particles is wave-particle interactions. The magnetosphere is extremely rich in the kinds of waves that it supports. It supports wave modes in a broad range of frequencies from 1 Hz to 100 MHz. Some of these modes (e.g., the whistler mode) can interact with energetic particles and scatter them in energy and pitch angle, the latter being the angle of inclination of the particle velocity vector with respect to the magnetic field direction. As a result of these perturbations some particles are precipitated out of the radiation belts and into the atmosphere where they are lost through collisions with the neutral gas.

The energetic charged particles execute three types of periodic motion:

1. a helical gyro motion around the static magnetic field lines,
2. mirroring motion (back and forth) between the northern and southern hemispheres
3. relatively slow drift around the Earth

A schematic of the radiation belts is shown in Figure 1.3. Typical energetic charged particle motion is depicted in Figure 1.4.

### **1.1.3. Wave-particle Interactions**

Wave particle interaction in the radiation belts can be classified as being either incoherent or coherent. The former includes incoherent wide-band electromagnetic wave interactions, which is the focus of the present study. In these interactions the forces exerted by the wave on the particle are uncorrelated, and the particle execute a random walk in the velocity space.

However, coherent interactions involve narrowband waves such as from ground transmitters, natural whistlers, triggered emissions and signals induced by large scale power grids. During such coherent interactions the wave induced forces are cumulative in nature, the particles therefore execute well defined motions and suffer significant perturbations in energy and momentum.

The purpose of the presented research is to study the nature of particle precipitation caused due to interaction between incoherent shear Alfvén wave noise and energetic charged particles in the radiation belts. Such a study will enable us to differentiate the effects of incoherent and coherent interaction on particles. This is important as one can expect low frequency noise to be present at low amplitudes all the time, and coherent interactions act only intermittently due to specific phenomena.

## **1.2. Review of Previous Work**

Considerable work has been done on the pitch angle scattering of radiation belt particles by electromagnetic waves [2], [3], [4], [5], [6], [7]. The idea in these works have been that the trapped particle population interacts through cyclotron resonance with electromagnetic disturbances along its orbit and is subjected to a series of scattering that are random in both direction and size. Hence the individual particles of the population undergo a random walk in pitch angle, and diffusion in equatorial pitch angle space results. This diffusion can then be studied by calculating the incoherent diffusion coefficients and solving a Fokker-Planck equation [8].

The current study, however, incorporates wave propagation characteristics obtained from realistic plasma parameters in the region of interest, and simulates the incoherent diffusion of the energetic particles by solving the relativistic Lorentz force equation through a test-particle approach. The study focuses specifically on low-frequency shear Alfvén wave mode. The propagation of this Alfvén wave mode through the plasmasphere has been modelled using 3D Finite Difference Time Domain (FDTD) solutions of the Linearized Magneto-hydrodynamic equations, by including the realistic plasma parameters. Other simulations of Alfvén wave propagation in the magnetosphere using FDTD has been carried out in the past decade [9] [10], however they do not attempt to study the Alfvén wave interaction with the radiation belt particles.

### **1.3. Outline of the Report**

This report is organized into five chapters:

Chapter 1 (current chapter) gives a brief introduction to the Earth's magnetosphere, radiation belts, and broad types of wave-particle interactions, and related research work previously conducted.

Chapter 2 explains the basic physics of the propagation of Alfvén waves in the magnetosphere, and its interaction with charged particles.

Chapter 3 describes the 3D FDTD simulations of wave propagation in Orthogonal Dipole Coordinates, and also the simulations of scattering of trapped charged particles due to shear-Alfvén wave noise in the plasmasphere.

Chapter 4 presents the results of the equatorial pitch angle scattering of the trapped charged particles in the radiation belts due to the interaction with shear-Alfvén wave noise modelled using realistic plasma parameters.

Chapter 5 summarizes the results presented in Chapter 4, and concludes with a discussion of future extensions to this work including suggestions for experimental validation.

### **1.4. Applications of the Present Work**

The Van Allen radiation belts are dynamic in nature, and understanding wave interaction with the energetic charge particle that it contains is essential to further understand its nature. The precipitated energetic particles from the radiation belts, can cause a variety of undesirable effects in spacecraft, components and biological systems. High energy electrons can cause dielectric charge build-up deep inside large space-crafts that may lead in turn to destructive arcing. High energy protons in the inner radiation belt are the main contributors to ionising dose deposition in shielded components in space-crafts.

The present work will help us understand the background pitch angle distribution of the radiation belt particles, and thereby understand the nature of the precipitated particles. Further extensions of this work can be used to identify the differences in the effect of scattering through incoherent and coherent wave-particle interaction.

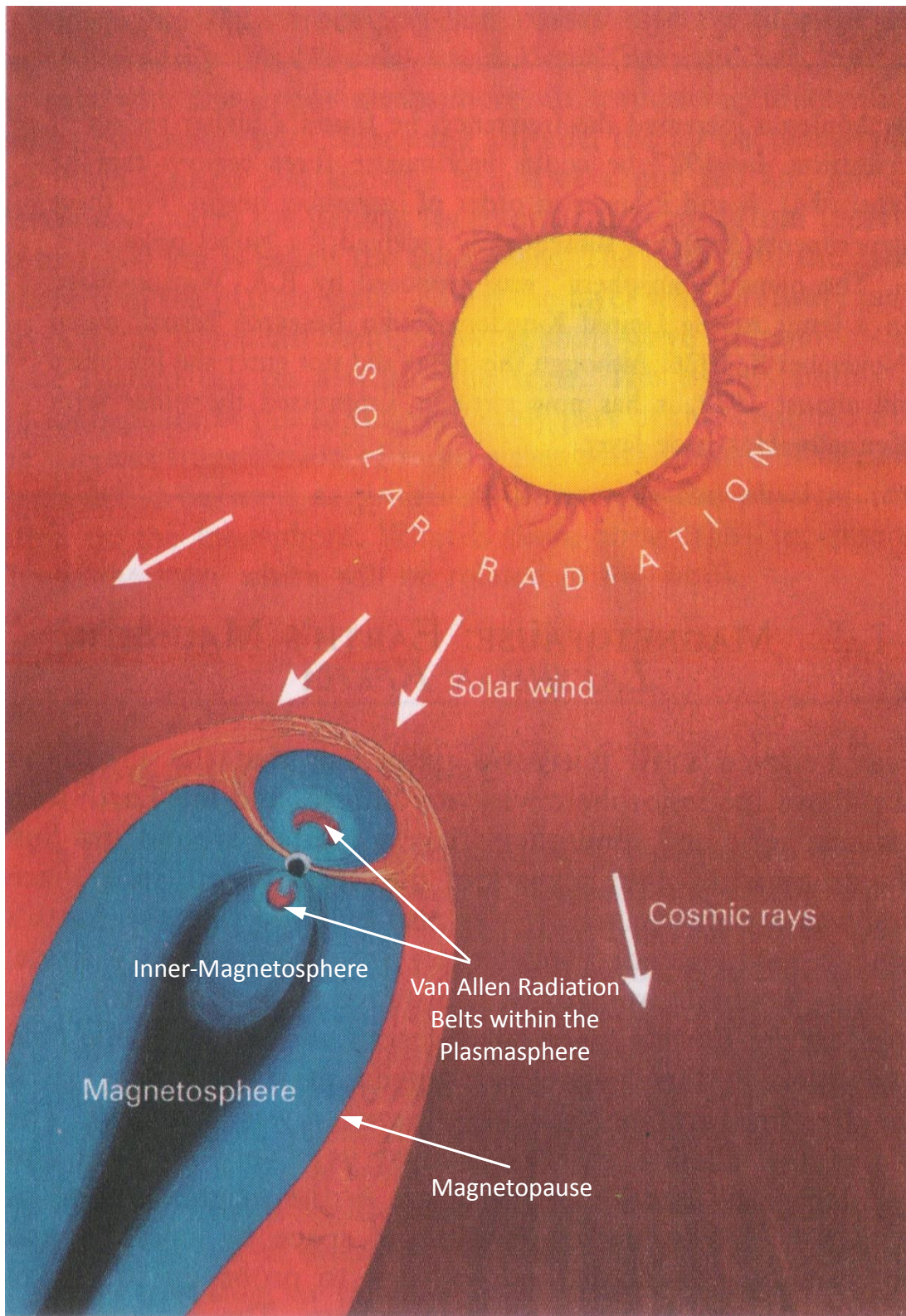


Figure 1.1: Earth's Magnetosphere being compressed by the solar wind and organized into a close cavity. (Illustrated by Eric A. Lord [11])

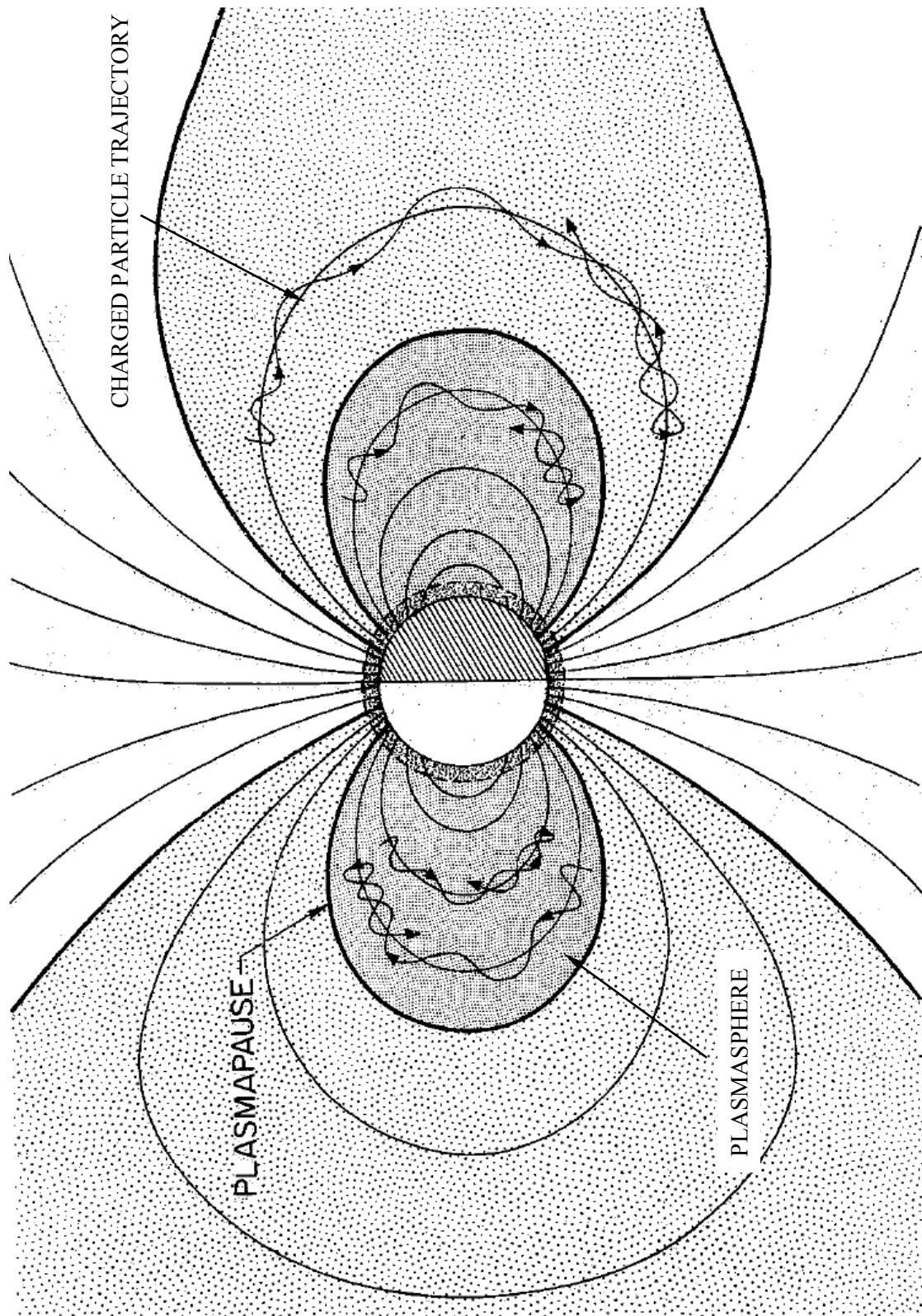


Figure 1.2: A cross section of the inner magnetosphere with dipole field lines, plasmasphere, plasmapause and the typical energetic charged particle trajectory along the field line. [12]

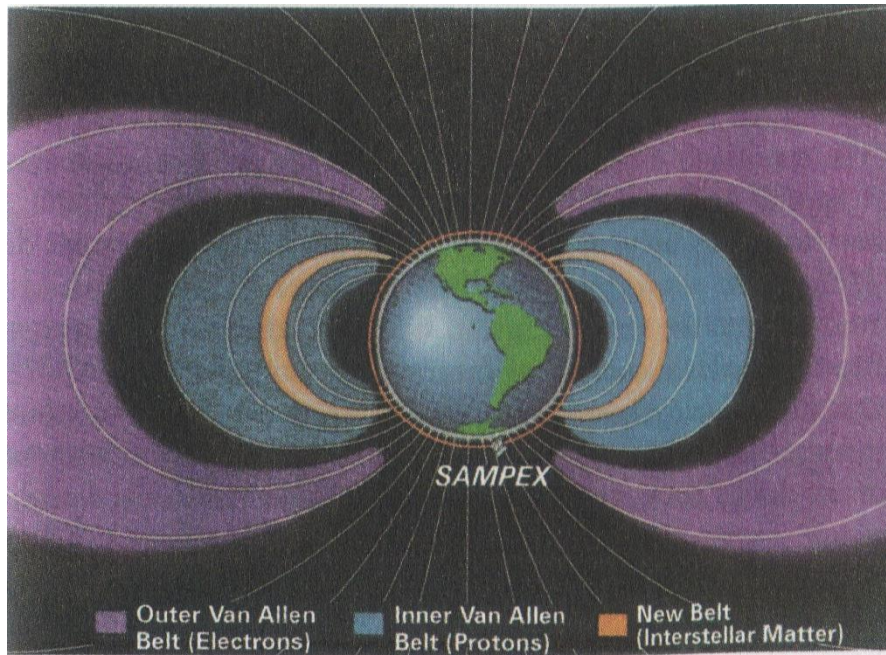


Figure 1.3: Schematic cross-section of the Van Allen Radiation Belts that surround the Earth. The inner belt is mainly composed of energetic protons, while the outer belt is mainly energetic electrons. A newly identified radiation belt is shown in Orange, is composed of energetic nuclei that originated in the local interstellar medium. The orbit of the polar orbiting SAMPEX satellite, which has been studying the new belt, is indicated. (R. A. Mewaldt, A.C. Cummings and E.C. Stone, EOS, 1994) [11]

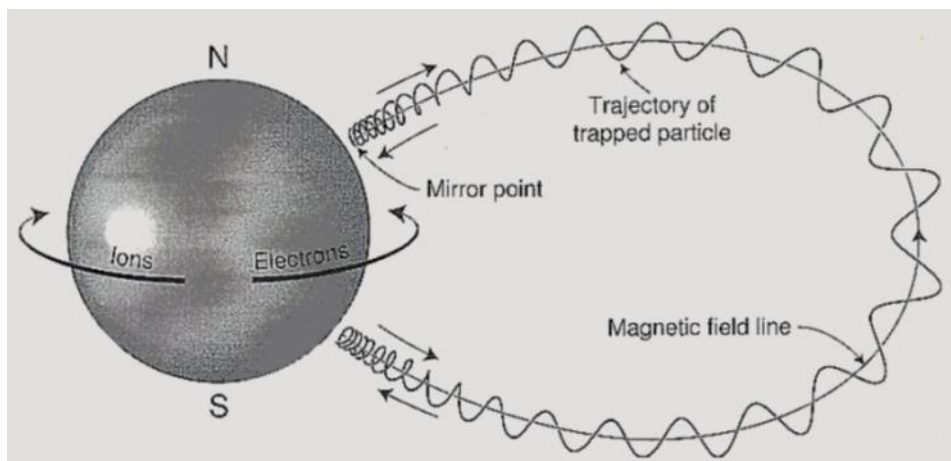


Figure 1.4: Typical trajectory of an energetic charged particle trapped within the geo-magnetic field. [13]

## CHAPTER 2

### 2. BASIC PHYSICS INVOLVED

This section provides the theoretical background necessary to understand the simulations and results described in the next two chapters. This section includes physics of low-frequency Alfvén wave propagation through magnetized plasma, motion of the trapped energetic charged particles in the radiation belts, and interaction of low frequency waves with these trapped charged particles.

#### 2.1. Low-Frequency Alfvén Wave Propagation through Magnetized Plasma

Consider low-frequency waves (i.e wave frequency ' $\omega$ '  $\ll$  ion cyclotron frequency ' $\omega_{ci}$ ') propagating in magnetized plasma i.e. a plasma immersed in magnetic field. These category of waves are known as Alfvén waves. These waves are the normal modes of MHD, involve magnetic perturbations, and have characteristic velocities of the order of the Alfvén velocity  $v_A = B/\sqrt{\mu_0\rho}$ . There are two distinct kinds of Alfvén waves. One mode is called the fast/compressional/magnetosonic mode ( $B_{\mu 1} = 0$ ) and the other slow/shear/Alfvén mode ( $B_{\mu 1} = 0$ ).

Assume,  $\mathbf{B} = B_0 \widehat{\mathbf{e}}_\mu$  ( $\widehat{\mathbf{e}}_\mu$  is directed along the magnetic field line in dipole coordinates)

We start with the linearized version of the Faraday's and Ampere's law.

$$\text{Faraday's Law : } \nabla \times \mathbf{E}_1 = -\frac{\partial \mathbf{B}_1}{\partial t} \dots \text{Eq. 2.1}$$

$$\text{Ampere's Law : } \nabla \times \mathbf{B}_1 = \mu_0 \mathbf{J}_1 + \mu_0 \epsilon_0 \frac{\partial \mathbf{E}_1}{\partial t} \dots \text{Eq. 2.2}$$

Here,  $\mathbf{B}(\mathbf{x}, t) = \mathbf{B}_0(\mathbf{x}) + \mathbf{B}_1(\mathbf{x}, t)$ , where  $|\mathbf{B}_1| \ll |\mathbf{B}_0|$  and similarly for the other quantities. In the present work we consider the zero-pressure MHD approximation, as it is suitable for low frequency waves and collision-less plasma. MHD essentially ignores parallel dynamics by invoking an ad hoc closure relation for the parallel current density in order to maintain overall current neutrality. The essence of the MHD modes comes from the polarization drift associated with a time-dependent perpendicular electric field namely,

$$u_{\sigma, \text{polarization}} = \frac{m_\sigma}{q_\sigma B^2} \frac{dE_\perp}{dt} \dots \text{Eq. 2.3 [14]}$$

The polarization drift results in a polarization current.

$$J_{\perp} = \sum n_{\sigma} q_{\sigma} \mathbf{u}_{\sigma, polarization} = \frac{\rho}{B^2} \frac{d\mathbf{E}_{\perp}}{dt} \dots Eq. 2.4$$

Where  $\rho = \sum n_{\sigma} m_{\sigma}$  is the mass density. Eq. 2.4 can be recast as

$$\therefore \frac{d\mathbf{E}_{\perp}}{dt} = \frac{B^2}{\mu_0 \rho} \mu_0 \mathbf{J}_{\perp} = v_A^2 (\nabla \times \mathbf{B})_{\perp} - v_A^2 \mu_0 \epsilon_0 \frac{\partial \mathbf{E}_{\perp}}{\partial t} \dots Eq. 2.5$$

where,  $v_A^2 = B^2 / \mu_0 \rho$  is the Alfven Velocity.

Simplifying further:  $\frac{d\mathbf{E}_{\perp}}{dt} = \frac{v_A^2}{(1 + v_A^2 \mu_0 \epsilon_0)} (\nabla \times \mathbf{B})_{\perp} \dots Eq. 2.6$ , we get the following:

$$\frac{d\mathbf{E}_{\perp}}{dt} = V_A^2 (\nabla \times \mathbf{B})_{\perp} \dots Eq. 2.7$$

Where,  $V_A^2 = c^2 v_A^2 / (c^2 + v_A^2) = 1 / (\epsilon_{\perp} \mu_0)$  and  $\epsilon_{\perp} = \epsilon_0 \left(1 + \frac{c^2}{v_A^2}\right)$

Eq. 2.1 and the linearized version of Eq. 2.7 give the two basic coupled equations governing the Alfven wave modes, namely:

$$\begin{aligned} \nabla \times \mathbf{E}_1 &= -\frac{\partial \mathbf{B}_1}{\partial t} \\ \frac{d\mathbf{E}_{\perp 1}}{dt} &= \frac{1}{\epsilon_{\perp} \mu_0} (\nabla \times \mathbf{B}_1)_{\perp} \quad \dots Eq. 2.8 \end{aligned}$$

$$where, \quad \epsilon_{\perp} = \epsilon_0 \left(1 + \frac{c^2}{v_A^2}\right)$$

For Slow , Shear or Alfven wave :  $\mathbf{B}_{\mu 1} = \mathbf{0}$

For Fast , Compressional or Magnetosonic wave :  $\mathbf{B}_{\mu 1} \neq \mathbf{0}$

Here  $B_{\mu 1}$  is the component of the wave's linearized magnetic field along the geo-magnetic field line (which is along the  $\mu$  axis in the orthogonal dipole coordinate system). Equation 2.8, cannot be solved analytically for spatially varying  $v_A$ . However, if  $v_A$  is constant the following simplified wave equations can be obtained for both the shear and compressional wave modes.

If  $\mathbf{B} = B_0 \hat{\mathbf{e}}_{\mu}$ ,

$$\begin{aligned} \text{Shear Alfven Wave : } \frac{\partial^2 \mathbf{B}_{\perp 1}}{\partial t^2} &= v_A^2 \frac{\partial^2 \mathbf{B}_{\perp 1}}{\partial z^2} \\ \text{Compressional Alfven Wave : } \frac{\partial^2 B_{\mu 1}}{\partial t^2} &= v_A^2 \nabla^2 B_{\mu 1} \end{aligned}$$

Comparing the dispersion relations:

$$\text{Shear Alfvén Wave: } \omega^2 = k_\mu^2 v_A^2$$

$$\text{Compressional Alfvén Wave: } \omega^2 = k^2 v_A^2$$

The above relations give us an idea about the basic differences in the nature of the two main Alfvén wave modes. In the magnetosphere, as  $v_A$  is spatially varying, the fields can only be solved for numerically/computationally.

## 2.2. Motion of Trapped Energetic Charged Particles in the Radiation Belt

The motion of a charge particle with charge  $q$  and mass  $m$  in an electric field  $\mathbf{E}$  and magnetic field  $\mathbf{B}$  can be described by the Newton-Lorentz equation:

$$\frac{d(\gamma m \mathbf{v})}{dt} = q\mathbf{E}(\mathbf{r}) + q \mathbf{v} \times \mathbf{B}(\mathbf{r}) \dots \text{Eq. 2.9}$$

Here  $\gamma = \left(1 - \frac{v^2}{c^2}\right)^{-\frac{1}{2}}$  is the relativistic factor and  $\mathbf{v}$  is the particle speed.

Suppose

$\mathbf{E} = 0$  (this is the case of the geo-magnetic field)

$\mathbf{B}$  is uniform

Then the acceleration of the particle is always perpendicular to the velocity, and so the speed of the particle (and the factor  $\gamma$ ) remains constant. These particles move on helical paths parallel to the field vector. The circular part of this motion is called the “cyclotron frequency”  $\Omega$  and the “cyclotron radius”  $\rho_\Omega$  are respectively given by:

$$\Omega = \frac{qB}{\gamma m}; \quad \rho_\Omega = \frac{\gamma m v_\perp}{qB}$$

Where  $B = |\mathbf{B}|$  is the uniform field strength and  $v_\perp$  is the component of the velocity perpendicular to the field vector. If there are no other forces, the parallel velocity component  $v_\parallel$  remains constant and hence the particle traces a helix with a pitch proportional to  $v_\parallel$ .

### 2.2.1. Magnetic Dipole

Now consider, a magnetic dipole field  $\mathbf{B}_{dip}(\mathbf{r})$  with moment vector  $\mathbf{M}$  at location  $\mathbf{r}$  given by

$$\mathbf{B}_{dip}(\mathbf{r}) = \frac{\mu_0}{4\pi r^3} [3(\mathbf{M} \cdot \hat{\mathbf{r}})\hat{\mathbf{r}} - \mathbf{M}]$$

Where  $\mathbf{r} = x \hat{\mathbf{e}}_x + y \hat{\mathbf{e}}_y + z \hat{\mathbf{e}}_z$ ,  $r = |\mathbf{r}|$  and  $\hat{\mathbf{r}} = \mathbf{r}/r$ . For Earth  $\mathbf{M} = -M\hat{\mathbf{e}}_z$ , as the magnetic north is the geographic south. Substituting this in the above equation we get,  $\mu_0 M/4\pi = B_0 R_E^3$ . Then the geo-magnetic field in Cartesian coordinates is given by:

$$B_{dip} = -\frac{B_0 R_E^3}{r^5} [3xz\hat{\mathbf{e}}_x + 3yz\hat{\mathbf{e}}_y + (2z^2 - x^2 - y^2)\hat{\mathbf{e}}_z] \dots \mathbf{Eq. 2.10}$$

At the magnetic equator ( $x = R_E, y = 0, z = 0$ ), the field strength is measured to be  $B_0 = 3.07 \times 10^{-5} T$ . Here  $R_E = 6.3712 \times 10^6 m$ , is the average radius of the Earth.

Figure 2.1 shows trajectories of two protons with a kinetic energy of 15 MeV (a typical energy of a proton within the radiation belt) with its starting point at  $(1.5R_E, 0, 0)$  and  $(4R_E, 0, 0)$ . Both start with an equatorial pitch angle of  $30^\circ$ , such that their velocities are defined as  $v_{0x} = 0, v_{0y} = v \sin \alpha_{eq}, v_{0z} = v \cos \alpha_{eq}$ . Both are followed through for 40 seconds.

### 2.2.2. The Three Kinds of Motion

The motion is mainly helical (i.e. cyclotron motion about the field line), but the non-uniformity of the field introduces the bounce and drift motions. The bounce motion is the periodic north-south oscillation along the field line that goes through the helix. This motion slows down as the particles moves towards locations with a stronger magnetic field, reflecting back at ‘‘mirror points’’. The bounce motion has a longer period than the cyclotron motion.

The pitch angle of the helix is the angle between the particle velocity and the magnetic field and is given by  $\alpha = \tan^{-1}(V_\perp/V_\parallel)$ . The magnetic moment of the gyrating particle can be shown to be a constant in the dipole magnetic field [1]. This requires  $(\sin^2 \alpha)/(B) = \text{constant}$ , and it enables us to determine the pitch angle of a particle at any point in the magnetic field line, provided you know the pitch angle and magnetic field of a reference point along the helical path of the gyrating particle. Since the dipole field is symmetric about the equator, knowing the equatorial pitch angle ( $\alpha_{eq}$ ) and the magnetic field line about which the particle gyrates becomes sufficient to determine the cyclotron and bounce motion of the particle.

The drift motion takes the particle around the Earth, perpendicular to the bounce motion and across the field lines. This motion is caused due to the gradient of the magnetic field along the particle’s path which results in a change in the gyro radius. Electrons and protons drift in opposite directions. In the geomagnetic field, protons drift westwards, electrons eastward. Particles in dipole-like fields are trapped on closed ‘drift shells’ as long as they are not disturbed by collisions or interactions with electromagnetic (EM) waves. The drift period is longer than the bounce period.

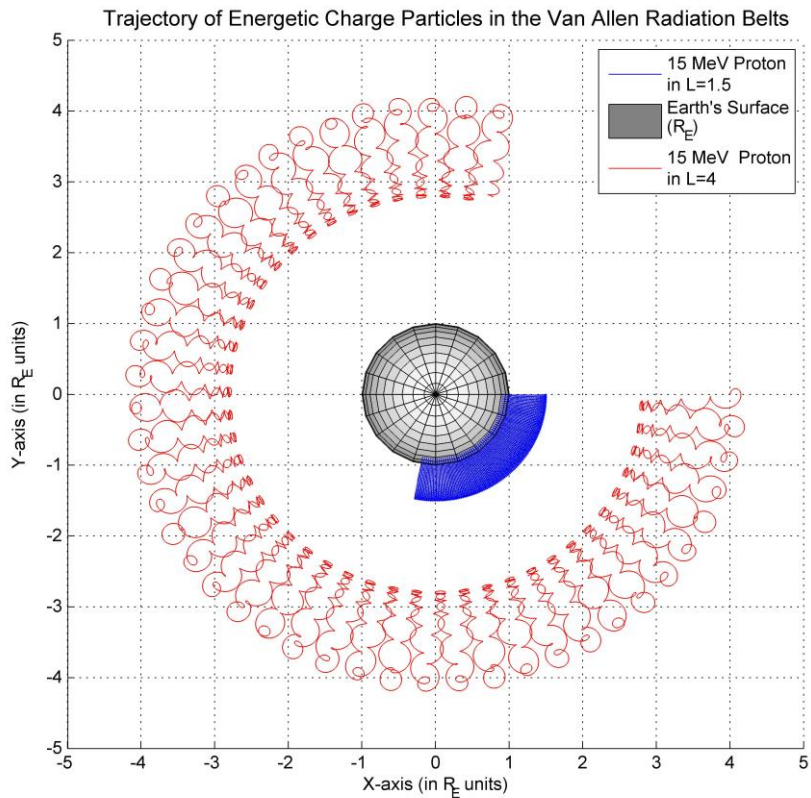
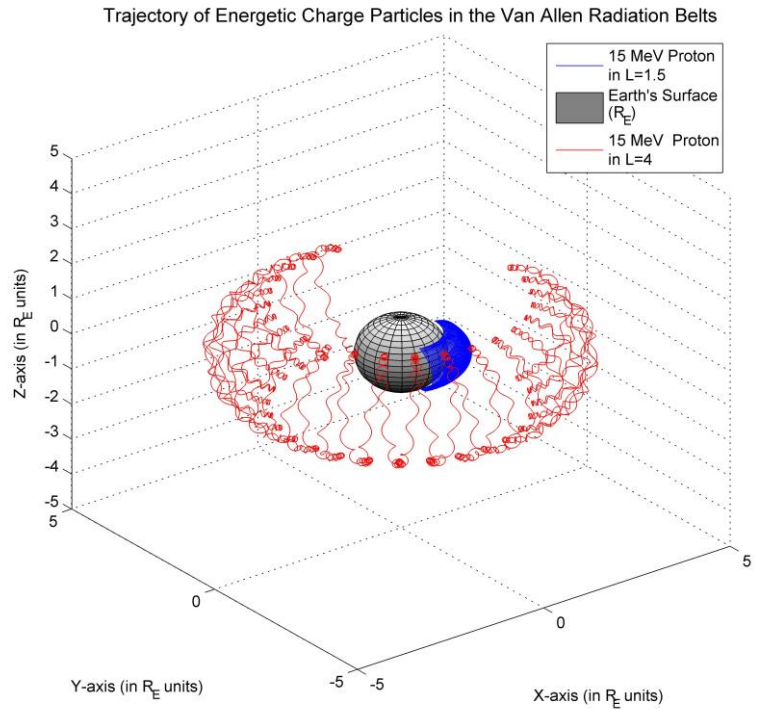


Figure 2.1: Trajectory of two protons of 15 MeV in the Earth's dipole magnetic field, generated by the 3-D Trajectory Solver described in Section 3.4 developed by the author. Isometric (above) and Top view (below) of the particle trajectories.

In a dipole field, the bounce motion period  $\tau_b$  and the drift motion  $\tau_d$  are approximately given by [1]

$$\tau_b \approx 0.117 \left( \frac{R_0}{R_E} \right) \frac{c}{v} \left[ 1 - 0.4635 (\sin \alpha_{eq})^{\frac{3}{4}} \right] \dots Eq. 2.11$$

$$\tau_d \approx \frac{2\pi q B_0 R_E^3}{m v^2} \left( \frac{1}{R_0} \right) \left[ 1 - \frac{1}{3} (\sin \alpha_{eq})^{0.62} \right] \dots Eq. 2.12$$

Here  $\alpha_{eq}$  is the equatorial pitch angle of the particle. Equatorial pitch angle can be used to calculate the mirror points of the particles in a dipole magnetic field. [15]

$$\sin^2 \alpha_{eq} = \frac{\sin^6 \theta_m}{\sqrt{1 + 3 \cos^2 \theta_m}} \dots Eq. 2.13$$

### 2.2.3. Loss cone angle

Particle with large pitch angles have mirror points located at high altitudes, and those with smaller pitch angles have mirror points at lower altitudes. If the pitch-angle is too small then the mirror points enter the Earth's atmosphere, and the particles are lost via collision with neutral particles. Neglecting the thickness of the atmosphere, we can say that all particles whose mirror points lie inside the Earth are lost via collisions. It follows from Eq. 2.13 that the *equatorial loss cone* [15] is approximately:

$$\sin^2 \alpha_l = \frac{\sin^6 \theta_E}{\sqrt{1 + 3 \cos^2 \theta_E}} \dots Eq. 2.13$$

Note that,

$$\begin{aligned} \sin^2 \theta_E &= L^{-1} \\ \Rightarrow \sin^2 \alpha_l &= (4L^6 - 3L^5)^{-0.5} \\ \Rightarrow \alpha_l &= \sin^{-1} (4L^6 - 3L^5)^{-0.25} \dots Eq. 2.14 \end{aligned}$$

### 2.3. Interaction of wave with particles in the radiation belts

There are several kinds of resonant interactions possible. However, the focus of the current study is not resonant interaction, but scattering of the particles in the velocity space due to shear-Alfven wave noise. Here we derive pitch angle scattering rates from simple physical arguments.

Note  $\tan \alpha = V_{\perp}/V_{\parallel}$ , and for large pitch angle particles where  $V_{\perp} \cong V$ , we have

$$\Delta\alpha = -\frac{\Delta V_{\parallel}}{V_{\perp}} \dots Eq. 2.15$$

The maximum change in the parallel velocity of a charged particle interacting with the electromagnetic wave is given by [16]

$$\Delta V_{\parallel} = \left(\frac{qV_{\perp}B_w}{m}\right)\Delta t \dots Eq. 2.16$$

$$\Delta\alpha = \frac{eB_w}{m}\Delta t \dots Eq. 2.17$$

Here  $B_w$  is the magnetic field of the EM wave. Equation 2.16 can be used to estimate the maximum pitch angle scattering that can occur due to EM wave interaction with particles.

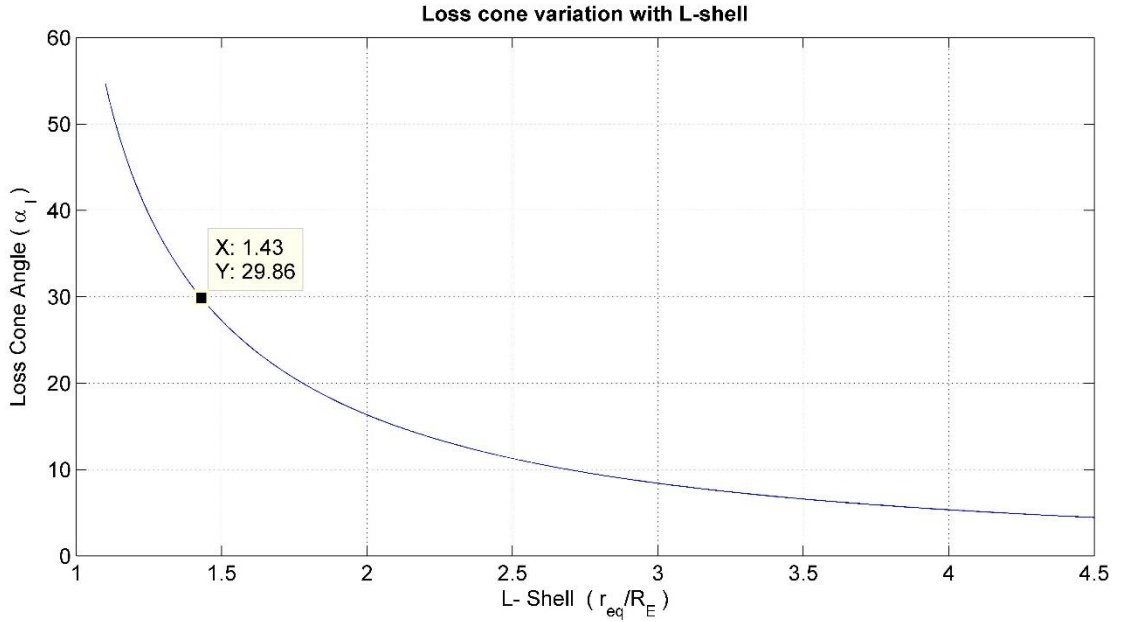


Figure 2.2: The variation of loss cone angle (equatorial pitch angle below which the particle is lost due to collision with the Earth's atmosphere) with respect to the McIlwain L coordinate, calculated using Eq. 2.14.

## CHAPTER 3

### 3. DESCRIPTION OF SIMULATIONS

This chapter presents the description of the simulations used for the current research. The objective of the simulations are to estimate the equatorial pitch angle scattering (or scattering in the velocity space) of trapped energetic charged particles in the radiation belts, due to its interaction with shear Alfvén wave noise. The following are the steps followed to achieve this objective:

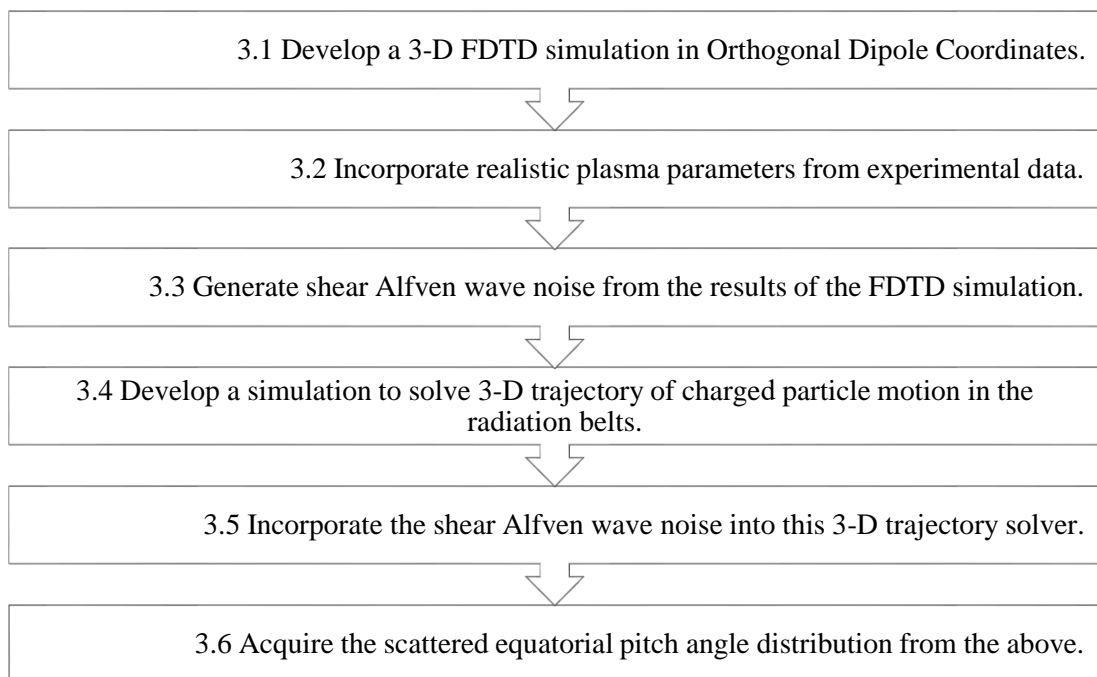


Figure 3.1: Flow chart of steps followed to attain the result

#### 3.1. 3-D FDTD Simulation in Orthogonal Dipole Coordinates

Finite Difference Time Domain (FDTD) method is widely used to solve electromagnetic wave propagation problems. In the present work the FDTD algorithm is implemented in 3D Orthogonal Dipole Coordinates. [9]

##### 3.1.1. Orthogonal Dipole Coordinate System

The orthogonal dipole coordinate system is a curvilinear coordinate system, like the spherical coordinates with its basis vectors orthogonal to each other at every point in the coordinate space. Dipole coordinates are useful in describing the propagation of MHD waves in the magnetosphere. There is a field aligned coordinate  $\mu$  that makes it easy to specify the magnetic

field intensity of the Geo-magnetic field, and also define the Alfvén wave velocity  $v_A$  (corresponding to the plasma density) at different altitudes in the magnetosphere.

However, a drawback is that the field aligned coordinate  $\mu$  does not correspond to a constant radial distance, except at the poles. Since the ionosphere, which constitutes the lower boundary of the region of interest, is largely controlled by gravity, it would be at constant radial distance. Therefore presently, the ionospheric boundary can be incorporated only with an accuracy limited by the grid size. However, for generating shear Alfvén wave noise confined to a particular magnetic field line, this issue does not pose any difficulty.

The Dipole coordinate system, consists of three mutually orthogonal coordinates:  $(\nu, \phi, \mu)$ . These coordinates are defined as follows:

$$\nu = -\frac{R_E \sin^2 \theta}{r}$$

$$\phi = \phi$$

$$\mu = \frac{R_E^2 \cos \theta}{r^2}$$

Note that the coordinates  $(\nu, \phi, \mu)$  are defined in terms of  $(r, \theta, \phi)$  – spherical coordinate system.

$R_E$  – radius of earth,  $\nu$  and  $\phi$  label a magnetic field line,  $\mu$  labels the position along the magnetic field line.

The coordinates  $(\nu, \phi, \mu)$  are also dimensionless. The unit vectors along these coordinates are as follows:

$$\hat{\nu} = \frac{\hat{r} \sin \theta - \hat{\theta} 2 \cos \theta}{\sqrt{1 + 3 \cos^2 \theta}} \quad \hat{\mu} = -\frac{\hat{r} 2 \cos \theta - \hat{\theta} \sin \theta}{\sqrt{1 + 3 \cos^2 \theta}} \quad \hat{\phi} = \hat{\phi}$$

The scale factors for the Dipole coordinate system is as follows:

$$h_\nu = \frac{r^2}{R_E \sin \theta \sqrt{1 + 3 \cos^2 \theta}}$$

$$h_{\phi} = r \sin \theta$$

$$h_\mu = \frac{r^3}{R_E^2 \sqrt{1 + 3 \cos^2 \theta}}$$

### 3.1.2. Simplified Maxwell's equation for Electromagnetic waves

$$\frac{\partial \mathbf{B}}{\partial t} = -\nabla \times \mathbf{E}$$

$$\frac{\partial \mathbf{E}}{\partial t} = \frac{1}{\mu_0 \epsilon_0} \nabla \times \mathbf{B}$$

The following Maxwell's equations for electromagnetic waves were first used to develop the 3-D FDTD algorithm in orthogonal dipole coordinate system. The equations were later modified to incorporate the MHD approximation necessary to model Alfvén wave propagation.

The above Maxwell's equations were transformed into the orthogonal dipole coordinate system as below:

$$\frac{\partial B_\nu}{\partial t} = -\frac{1}{h_\phi h_\mu} \left[ h_\mu \frac{\partial E_\mu}{\partial \phi} - h_\phi \frac{\partial E_\phi}{\partial \mu} \right];$$

$$\frac{\partial B_\phi}{\partial t} = -\frac{1}{h_\mu h_\nu} \left[ h_\nu \frac{\partial E_\nu}{\partial \mu} - h_\mu \frac{\partial E_\mu}{\partial \nu} \right];$$

$$\frac{\partial B_\mu}{\partial t} = -\frac{1}{h_\nu h_\phi} \left[ h_\phi \frac{\partial E_\phi}{\partial \nu} - h_\nu \frac{\partial E_\nu}{\partial \phi} \right]$$

$$\frac{\partial E_\nu}{\partial t} = \frac{c^2}{h_\phi h_\mu} \left[ h_\mu \frac{\partial B_\mu}{\partial \phi} - h_\phi \frac{\partial B_\phi}{\partial \mu} \right];$$

$$\frac{\partial E_\phi}{\partial t} = \frac{c^2}{h_\mu h_\nu} \left[ h_\nu \frac{\partial B_\nu}{\partial \mu} - h_\mu \frac{\partial B_\mu}{\partial \nu} \right];$$

$$\frac{\partial E_\mu}{\partial t} = \frac{c^2}{h_\nu h_\phi} \left[ h_\phi \frac{\partial B_\phi}{\partial \nu} - h_\nu \frac{\partial B_\nu}{\partial \phi} \right]$$

Note:

$$\nabla \times \mathbf{A} = \frac{1}{h_\nu h_\phi h_\mu} \begin{vmatrix} h_\nu \widehat{e}_\nu & h_\phi \widehat{e}_\phi & h_\mu \widehat{e}_\mu \\ \frac{\partial}{\partial \nu} & \frac{\partial}{\partial \phi} & \frac{\partial}{\partial \mu} \\ h_\nu A_\nu & h_\phi A_\phi & h_\mu A_\mu \end{vmatrix}$$

### 3.1.3. Discretization of the Maxwell's equation

These equations were discretised over time and space as follows by the author:

$$B_v \Big|_{v, \phi + \frac{1}{2}, \mu + \frac{1}{2}}^{n + \frac{1}{2}} = B_v \Big|_{v, \phi + \frac{1}{2}, \mu + \frac{1}{2}}^{n - \frac{1}{2}} - \frac{\Delta t}{[h_\phi h_\mu]_{v, \phi + \frac{1}{2}, \mu + \frac{1}{2}}} \left[ \frac{[h_\mu E_\mu]_{v, \phi + 1, \mu + \frac{1}{2}}^n - [h_\mu E_\mu]_{v, \phi, \mu + \frac{1}{2}}^n}{\Delta \phi} - \frac{[h_\phi E_\phi]_{v, \phi + \frac{1}{2}, \mu + 1}^n - [h_\phi E_\phi]_{v, \phi + \frac{1}{2}, \mu}^n}{\Delta \mu} \right]$$

$$B_\phi \Big|_{v + \frac{1}{2}, \phi, \mu + \frac{1}{2}}^{n + \frac{1}{2}} = B_\phi \Big|_{v + \frac{1}{2}, \phi, \mu + \frac{1}{2}}^{n - \frac{1}{2}} - \frac{\Delta t}{[h_\mu h_\nu]_{v + \frac{1}{2}, \phi, \mu + \frac{1}{2}}} \left[ \frac{[h_\nu E_\nu]_{v + \frac{1}{2}, \phi, \mu + 1}^n - [h_\nu E_\nu]_{v + \frac{1}{2}, \phi, \mu}^n}{\Delta \mu} - \frac{[h_\mu E_\mu]_{v + 1, \phi, \mu + \frac{1}{2}}^n - [h_\mu E_\mu]_{v, \phi, \mu + \frac{1}{2}}^n}{\Delta v} \right]$$

$$B_\mu \Big|_{v + \frac{1}{2}, \phi + \frac{1}{2}, \mu}^{n + \frac{1}{2}} = B_\mu \Big|_{v + \frac{1}{2}, \phi + \frac{1}{2}, \mu}^{n - \frac{1}{2}} - \frac{\Delta t}{[h_\nu h_\phi]_{v + \frac{1}{2}, \phi + \frac{1}{2}, \mu}} \left[ \frac{[h_\phi E_\phi]_{v + 1, \phi + \frac{1}{2}, \mu}^n - [h_\phi E_\phi]_{v, \phi + \frac{1}{2}, \mu}^n}{\Delta v} - \frac{[h_\nu E_\nu]_{v + \frac{1}{2}, \phi + 1, \mu}^n - [h_\nu E_\nu]_{v + \frac{1}{2}, \phi, \mu}^n}{\Delta \phi} \right]$$

$$E_\nu \Big|_{v + \frac{1}{2}, \phi, \mu}^{n + 1} = E_\nu \Big|_{v + \frac{1}{2}, \phi, \mu}^n + \frac{c^2 \Delta t}{[h_\phi h_\mu]_{v + \frac{1}{2}, \phi, \mu}} \left[ \frac{[h_\mu B_\mu]_{v + \frac{1}{2}, \phi + \frac{1}{2}, \mu}^{n + \frac{1}{2}} - [h_\mu B_\mu]_{v + \frac{1}{2}, \phi - \frac{1}{2}, \mu}^{n + \frac{1}{2}}}{\Delta \phi} - \frac{[h_\phi B_\phi]_{v + \frac{1}{2}, \phi, \mu + \frac{1}{2}}^{n + \frac{1}{2}} - [h_\phi B_\phi]_{v + \frac{1}{2}, \phi, \mu - \frac{1}{2}}^{n + \frac{1}{2}}}{\Delta \mu} \right]$$

$$\begin{aligned}
E_\phi|_{\nu, \phi + \frac{1}{2}, \mu}^{n+1} &= E_\phi|_{\nu, \phi + \frac{1}{2}, \mu}^n \\
&+ \frac{c^2 \Delta t}{[h_\mu h_\nu]_{\nu, \phi + \frac{1}{2}, \mu}} \left[ \frac{[h_\nu B_\nu]_{\nu, \phi + \frac{1}{2}, \mu + \frac{1}{2}}^{n+\frac{1}{2}} - [h_\nu B_\nu]_{\nu, \phi + \frac{1}{2}, \mu - \frac{1}{2}}^{n+\frac{1}{2}}}{\Delta \mu} \right. \\
&\quad \left. - \frac{[h_\mu B_\mu]_{\nu + \frac{1}{2}, \phi + \frac{1}{2}, \mu}^{n+\frac{1}{2}} - [h_\mu B_\mu]_{\nu - \frac{1}{2}, \phi + \frac{1}{2}, \mu}^{n+\frac{1}{2}}}{\Delta \nu} \right]
\end{aligned}$$

$$\begin{aligned}
E_\mu|_{\nu, \phi, \mu + \frac{1}{2}}^{n+1} &= E_\mu|_{\nu, \phi, \mu + \frac{1}{2}}^n \\
&+ \frac{c^2 \Delta t}{[h_\nu h_\phi]_{\nu, \phi, \mu + \frac{1}{2}}} \left[ \frac{[h_\phi B_\phi]_{\nu + \frac{1}{2}, \phi, \mu + \frac{1}{2}}^{n+\frac{1}{2}} - [h_\phi B_\phi]_{\nu - \frac{1}{2}, \phi, \mu + \frac{1}{2}}^{n+\frac{1}{2}}}{\Delta \nu} \right. \\
&\quad \left. - \frac{[h_\nu B_\nu]_{\nu, \phi + \frac{1}{2}, \mu + \frac{1}{2}}^{n+\frac{1}{2}} - [h_\nu B_\nu]_{\nu, \phi - \frac{1}{2}, \mu + \frac{1}{2}}^{n+\frac{1}{2}}}{\Delta \phi} \right]
\end{aligned}$$

Here,  $n$  refers to time instant and  $\nu, \phi, \mu$  refers to the spatial locations. In FDTD the  $E$ -fields and  $B$ -fields cells in the simulation grids are interleaved in both space and time. And hence,  $n + 1, n + \frac{1}{2}$  refers to the new value of time and  $n - 1, n - \frac{1}{2}$  refers to the previous value of time in a particular time-step  $n$ . Similarly  $\nu + 1, \nu + \frac{1}{2}$  refers to the grid-cell towards the positive direction and  $\nu - 1, \nu - \frac{1}{2}$  refers to the grid-cell towards the negative direction with respect to the current grid-cell  $\nu$  in a particular time-step iteration.

The above set of discretized equations are solved to obtain the field strengths in MATLAB by placing a source at a desirable location in the grid, and with the desired temporal variation and polarization. The performance of the simulations with the equations discretized in 3-D Dipole coordinates has *not* been compared with discretization in 3-D Cartesian coordinates in this work.

Figure 3.2 and 3.3 shows the FDTD simulation grid in Orthogonal Dipole Coordinate Systems.

Figure 3.4 and 3.5 shows an EM wave originating from a line source in  $\mu = 0$  plane with fields constant along  $\phi$  i.e.  $\left(\frac{\partial}{\partial \phi} = 0\right)$ , propagating in Vacuum and spreading isotropically outward in  $\phi = 0$  plane as expected.

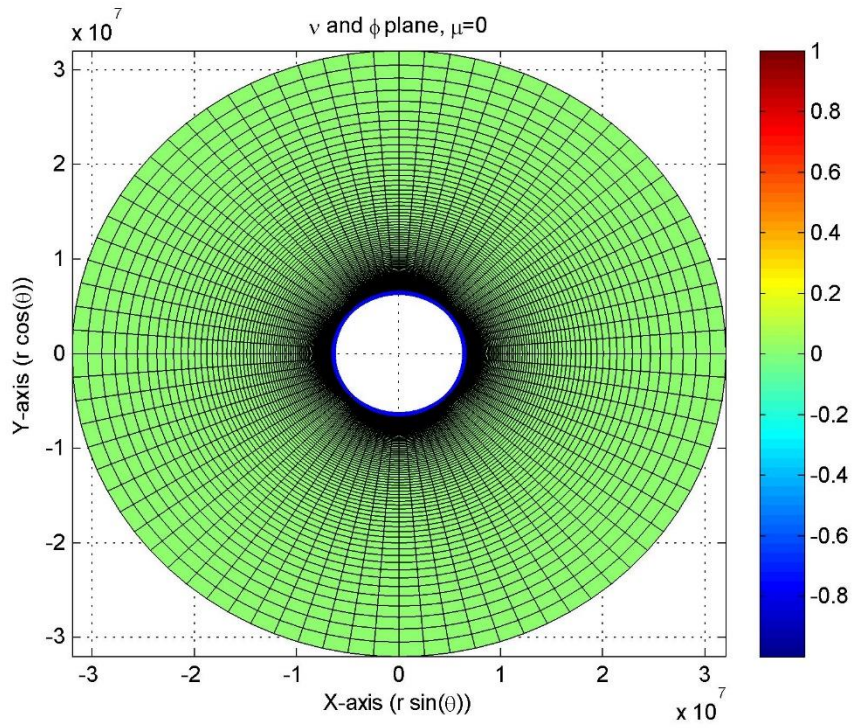


Figure.2: Plane  $\mu=0$ . Top view of the plasmasphere. Blue circle in the centre represents the Earth.

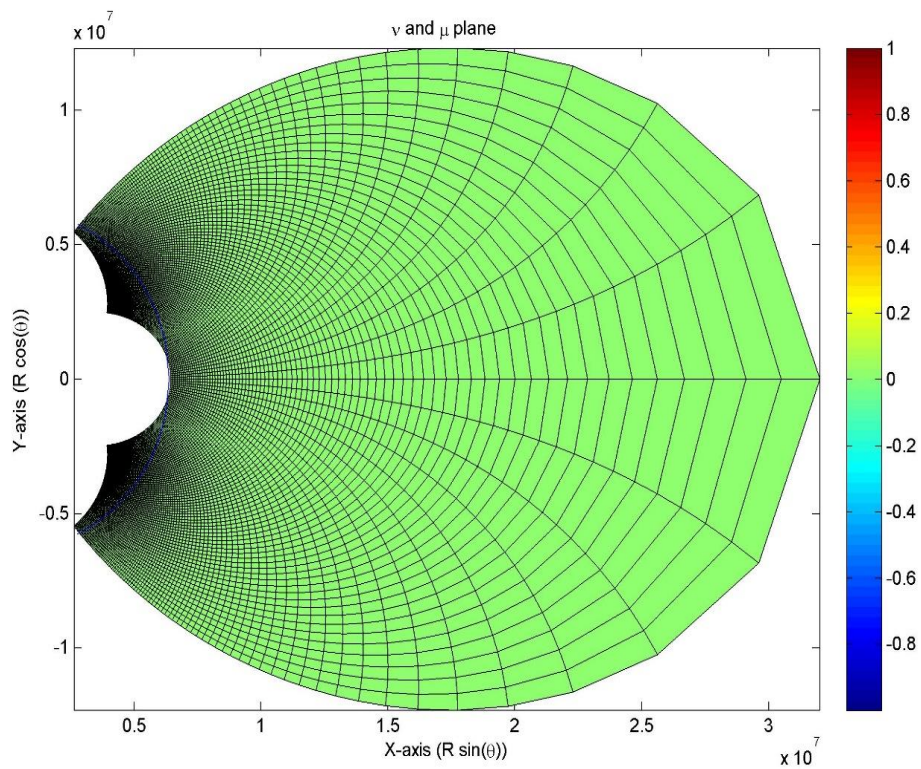


Figure 3.3: Plane  $\phi=0$ . Cross sectional view of the plasmasphere. Blue semi-circle towards the left-side of the figure represents one-half of the Earth.

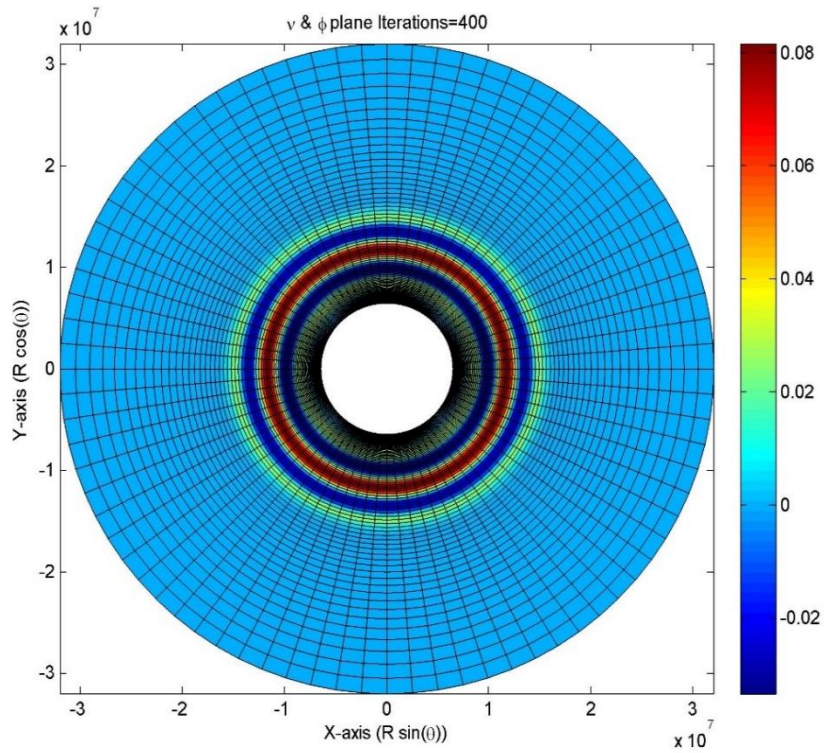


Figure 3.4: Plane  $\mu = 0$ . EM source with  $E_\phi$  polarization, and  $\frac{\partial}{\partial\phi} = 0$ .

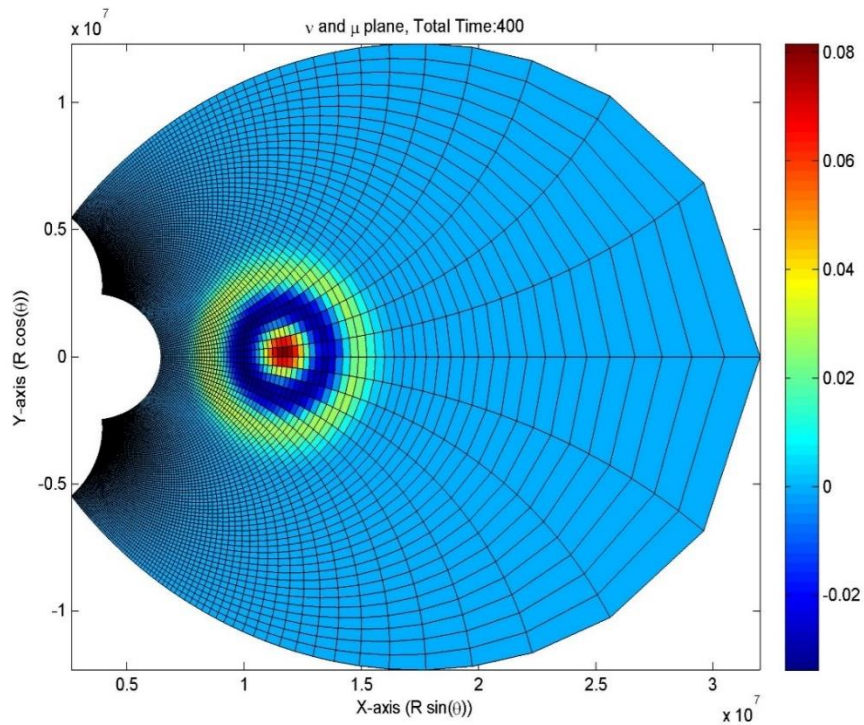


Figure 3.5: Plane  $\phi=0$ . EM source with  $E_\phi$  polarization. EM wave originating from a line source in  $\mu = 0$  plane with  $\frac{\partial}{\partial\phi} = 0$ , propagating in Vacuum and spreading isotropically outward in  $\phi = 0$  plane as expected.

### 3.1.4. Linearized MHD Equations

The FDTD algorithm can be modified to incorporate the Linearized MHD Equations, by replacing  $\epsilon_0$  with  $\epsilon_\perp$ . [9]

$$\frac{\partial \mathbf{B}}{\partial t} = -\nabla \times \mathbf{E}; \quad \frac{\partial \mathbf{E}_\perp}{\partial t} = \frac{1}{\mu_0 \epsilon_\perp} \nabla \times \mathbf{B}; \quad \mathbf{E}_\parallel = \mathbf{0}$$

$$\epsilon_\perp = \epsilon_0 \left( 1 + \frac{c^2}{v_A^2} \right); \quad v_A = \frac{B_0}{\sqrt{\mu_0 \rho}}; \quad V_A = \frac{1}{\mu_0 \epsilon_\perp}$$

The equations are discretized in Orthogonal Dipole Coordinates in a manner similar to Section 3.1.3. The only difference is that  $c$  is replaced by  $V_A$  and  $E_\mu$  set to 0 as per the Linearized MHD approximation.

$$B_v \Big|_{v, \phi + \frac{1}{2}, \mu + \frac{1}{2}}^{n + \frac{1}{2}} = B_v \Big|_{v, \phi + \frac{1}{2}, \mu + \frac{1}{2}}^{n - \frac{1}{2}} - \frac{\Delta t}{[h_\phi h_\mu]_{v, \phi + \frac{1}{2}, \mu + \frac{1}{2}}} \left[ \frac{[h_\phi E_\phi]_{v, \phi + \frac{1}{2}, \mu + 1}^n - [h_\phi E_\phi]_{v, \phi + \frac{1}{2}, \mu}^n}{\Delta \mu} \right]$$

$$B_\phi \Big|_{v + \frac{1}{2}, \phi, \mu + \frac{1}{2}}^{n + \frac{1}{2}} = B_\phi \Big|_{v + \frac{1}{2}, \phi, \mu + \frac{1}{2}}^{n - \frac{1}{2}} - \frac{\Delta t}{[h_\mu h_v]_{v + \frac{1}{2}, \phi, \mu + \frac{1}{2}}} \left[ \frac{[h_v E_v]_{v + \frac{1}{2}, \phi, \mu + 1}^n - [h_v E_v]_{v + \frac{1}{2}, \phi, \mu}^n}{\Delta \mu} \right]$$

$$B_\mu \Big|_{v + \frac{1}{2}, \phi + \frac{1}{2}, \mu}^{n + \frac{1}{2}} = B_\mu \Big|_{v + \frac{1}{2}, \phi + \frac{1}{2}, \mu}^{n - \frac{1}{2}} - \frac{\Delta t}{[h_v h_\phi]_{v + \frac{1}{2}, \phi + \frac{1}{2}, \mu}} \left[ \frac{[h_\phi E_\phi]_{v + 1, \phi + \frac{1}{2}, \mu}^n - [h_\phi E_\phi]_{v, \phi + \frac{1}{2}, \mu}^n}{\Delta v} - \frac{[h_v E_v]_{v + \frac{1}{2}, \phi + 1, \mu}^n - [h_v E_v]_{v + \frac{1}{2}, \phi, \mu}^n}{\Delta \phi} \right]$$

$$E_v \Big|_{v + \frac{1}{2}, \phi, \mu}^{n + 1} = E_v \Big|_{v + \frac{1}{2}, \phi, \mu}^n + \frac{V_A^2 \Delta t}{[h_\phi h_\mu]_{v + \frac{1}{2}, \phi, \mu}} \left[ \frac{[h_\mu B_\mu]_{v + \frac{1}{2}, \phi + \frac{1}{2}, \mu}^{n + \frac{1}{2}} - [h_\mu B_\mu]_{v + \frac{1}{2}, \phi - \frac{1}{2}, \mu}^{n + \frac{1}{2}}}{\Delta \phi} - \frac{[h_\phi B_\phi]_{v + \frac{1}{2}, \phi, \mu + \frac{1}{2}}^{n + \frac{1}{2}} - [h_\phi B_\phi]_{v + \frac{1}{2}, \phi, \mu - \frac{1}{2}}^{n + \frac{1}{2}}}{\Delta \mu} \right]$$

$$E_{\phi} \Big|_{\nu, \phi + \frac{1}{2}, \mu}^{n+1} = E_{\phi} \Big|_{\nu, \phi + \frac{1}{2}, \mu}^n + \frac{V_A^2 \Delta t}{[h_{\mu} h_{\nu}]_{\nu, \phi + \frac{1}{2}, \mu}} \left[ \frac{[h_{\nu} B_{\nu}]_{\nu, \phi + \frac{1}{2}, \mu + \frac{1}{2}}^{n+\frac{1}{2}} - [h_{\nu} B_{\nu}]_{\nu, \phi + \frac{1}{2}, \mu - \frac{1}{2}}^{n+\frac{1}{2}}}{\Delta \mu} - \frac{[h_{\mu} B_{\mu}]_{\nu + \frac{1}{2}, \phi + \frac{1}{2}, \mu}^{n+\frac{1}{2}} - [h_{\mu} B_{\mu}]_{\nu - \frac{1}{2}, \phi + \frac{1}{2}, \mu}^{n+\frac{1}{2}}}{\Delta \nu} \right]$$

### 3.2. Acquiring Realistic Plasma Parameters

In order to estimate the realistic value of  $v_A$ , Alfven wave velocity, realistic values for  $B_0$  (magnetic field) and  $\rho$  (plasma densities) obtained from existing models.

#### 3.2.1. Magnetic Field Intensity

The International Geomagnetic Reference Field (IGRF) Model was used to acquire the realistic value of the magnetic field in regions of interest. A MATLAB function, *igrf* [17], capable of returning the magnetic field vector, at a particular time and position was used. (See Figure 3.6 and 3.7)

#### 3.2.2. Plasma Density

The electron and proton plasma densities have been acquired from the Global Core Plasma Model (GCPM) Version 2.4. [18] The model is capable of returning values of proton, electron, helium and oxygen densities in the magnetosphere, for the specific time, location, and planetary  $k_p$  index number. A FORTRAN code was written to extract data from the GCPM ver. 2.4. (See Figure 3.8 and 3.9)

#### 3.2.3. Alfven Wave Velocity

From the acquired magnetic field intensity and plasma density, we can calculate the Alfven wave velocity in the regions of interest. (See Figure 3.10 and 3.11). Note that the Alfven wave velocity  $v_A$  is not defined in the regions where plasma density  $\rho$  is zero.

$$v_A = \frac{B_0}{\sqrt{\mu_0 \rho}} \dots Eq. 3.1$$

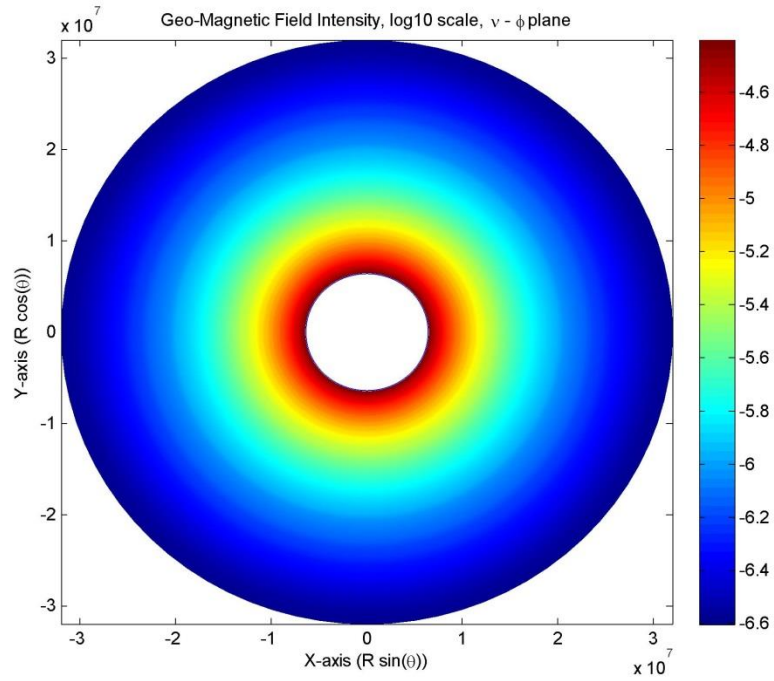


Figure 3.6: Plane  $\mu = 0$ . Magnetic field intensity ( $B_0$ ) in log scale.

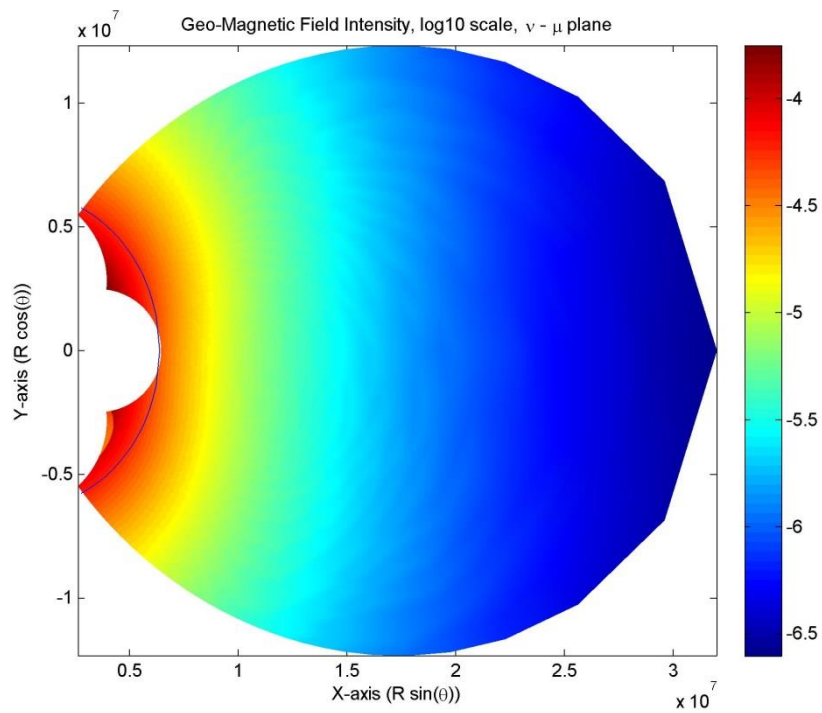


Figure 3.7: Plane  $\phi=0$ . Magnetic field intensity ( $B_0$ ) in log scale.

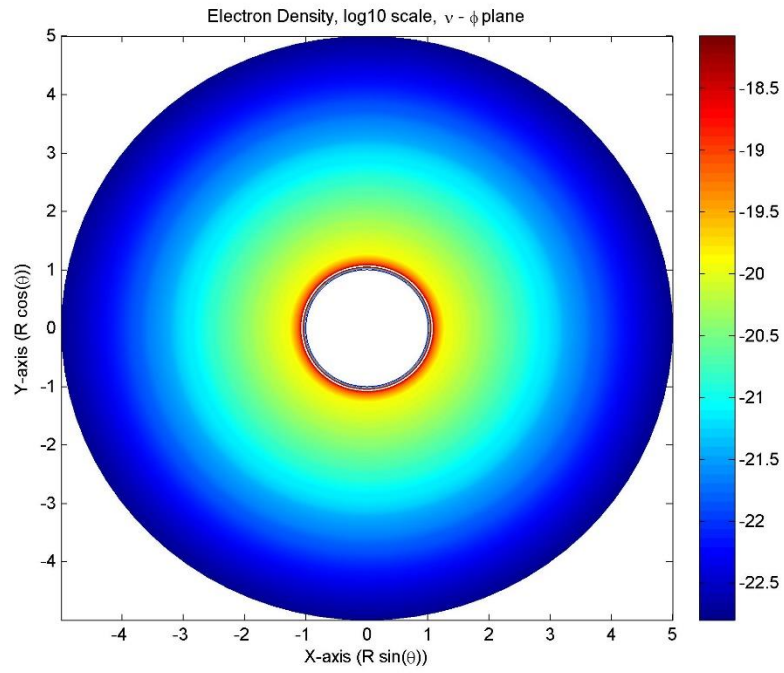


Figure 3.8: Plane  $\mu=0$ . Electron (plasma) density ( $\rho$ ) in log scale.

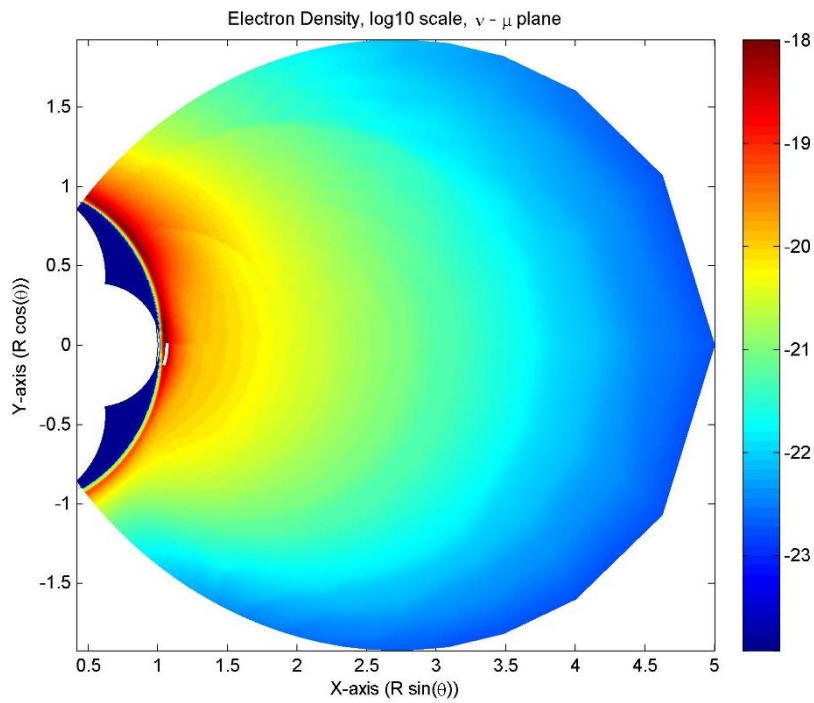


Figure 3.9: Plane  $\phi=0$ . Electron (plasma) density ( $\rho$ ) in log scale.

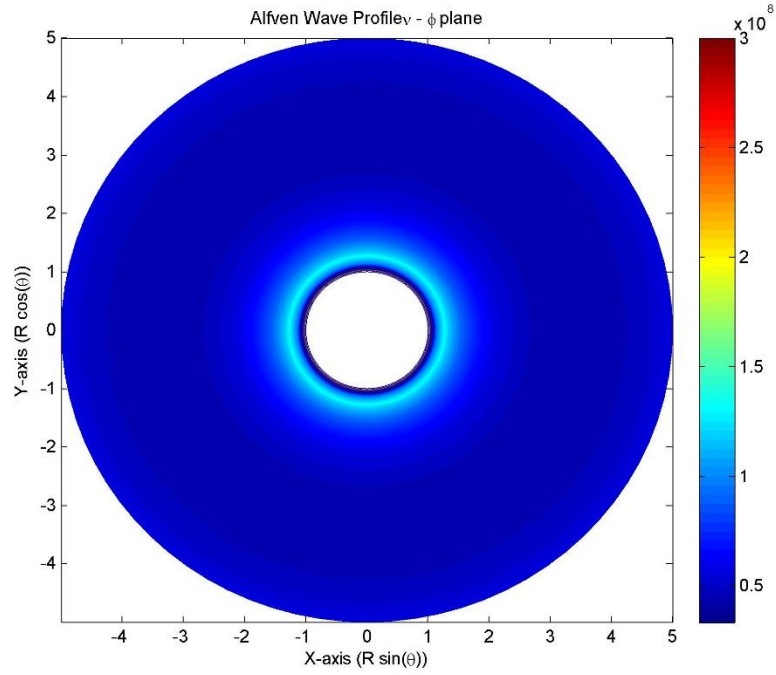


Figure 3.10: Plane  $\mu=0$ . Alfven wave velocity ( $v_A$ ) in log scale.

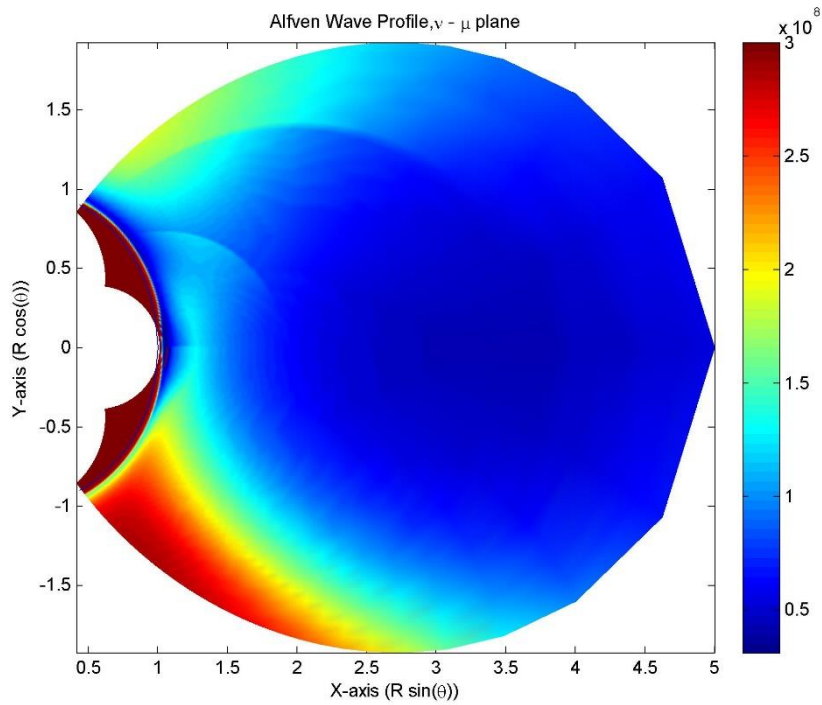


Figure 3.11: Plane  $\phi=0$ . Alfven wave velocity ( $v_A$ ) in log scale.

### 3.3. Generate Shear Alfvén Wave Noise

#### 3.3.1. Sinusoidal Shear-Alfvén Wave

In the MHD limit, it is assumed that there is no parallel electric field (parallel to the magnetic field line). This approximation yields two wave modes: 1. Slow/Shear/Alfvén wave mode ( $B = B_{\perp}; B_{\parallel} = 0$ ) and 2. Fast/Compressional/Magnetosonic mode ( $B = B_{\parallel}, B_{\parallel} \neq 0$ ). Example of a Shear Alfvén wave mode propagating along the magnetic field line obtained using the 3-D FDTD Simulations in Dipole Coordinates is shown in Figure 3.12.

In Figure 3.12, the black lines define the boundaries of the simulation space, beyond which Perfectly Matched Layers (PML), with artificial conductivities are incorporated to absorb the wave and prevent it from reflecting back into the simulation space. The hemispherical black boundary line with radius  $1 R_E$ , represents the Earth's surface. In this figure, a sinusoidal source (which is a line-source in  $\mu = 0$  plane, with its length along  $\phi$  direction) is placed about 300 km above the Earth's surface, where the ionosphere plasma density is highest. The wave propagates upwards and downwards along the magnetic field line. The wave propagating downwards into the Earth's neutral atmosphere and ground is absorbed by the PML, thereby stopping it from reflecting back into the simulation space. The simulation is stopped before the wave reaches the southern ionosphere boundary.

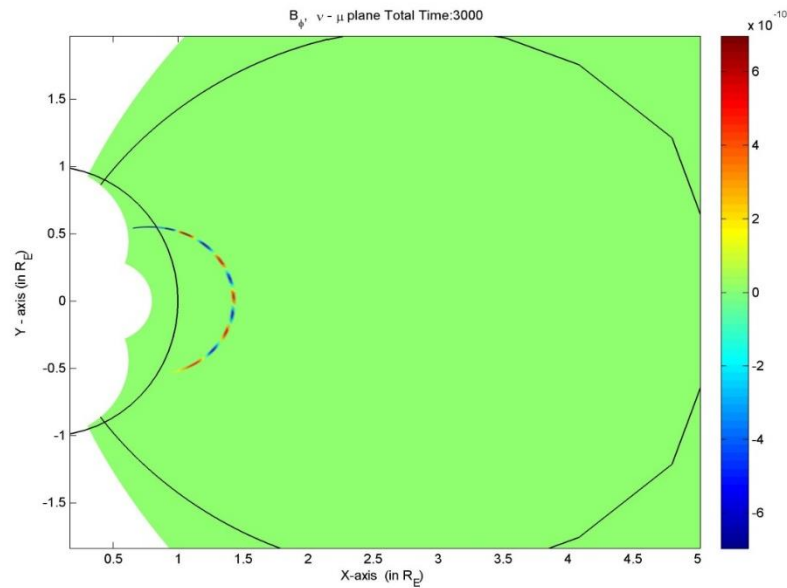


Figure 3.12: Shear-Alfvén-wave mode with sinusoidal source polarized in  $B_{\phi}$  ( $B_{\phi}$  is  $\perp$  to the magnetic field line and  $k$  vector of the wave)

### 3.3.2. Dispersion Diagram of a Shear-Alfven Wave in the Plasmasphere

Now, a Discrete Space-Time Fast Fourier transform (DFFT) is implemented on the Shear-Alfven Wave signal that is travelling along the magnetic field line. The source signal was a Gaussian pulse with a bandwidth of 6000 Hz, centred at a frequency of 3000 Hz. The DFFT is done over the spatial distance ' $s$ ' along the field line, and time ' $t$ '.

Here, we should note that the space-time DFFT cannot be applied directly over the signal extracted from the FDTD simulation, as the signal is a function of  $(\mu, t)$ . The signal should be transformed into  $(s, t)$ . This was done by converting the  $\mu$  sample points to corresponding distance ' $s$ ' by multiplying it with the appropriate scale factor  $h_\mu$ . These sample ' $s$ ' points are not uniform, i.e. the difference between each sample is unequal. For an accurate DFFT, the sample points must be equidistant from each other. This was done by doing spline interpolation of the signal at sample points which were equidistant from each other, from the existing data interspaced at uneven distances. The space-time DFFT was then applied to this transformed signal to get the fields in the Fourier domain  $(\omega, k)$ .

Discrete Space-Time Fourier Transform can be represented with the following equation:

$$B(\omega, \kappa) = \sum_{s=0}^{M-1} \sum_{t=0}^{N-1} B(s, t) e^{-i2\pi\kappa s/M} e^{-i2\pi\omega t/N} \Delta t \Delta s$$

Here  $\kappa$  is the wave number,  $\omega$  is the frequency, and N and M are the number of time and space samples respectively.

The signal which is used for the Space-Time DFFT is as long as 0.077 seconds, enough to reach the ionosphere boundary starting from the equatorial plane ( $\mu = 0$ ). **The ionosphere boundary condition is set to be perfectly reflecting.**

Figure 3.13 is the dispersion diagram of a Shear-Alfven Wave propagating along the magnetic field line with  $L=1.4286$ . It is produced by taking the Discrete Space-Time Fast Fourier Transform of the signal  $(B_\phi(s, t))$  and normalizing it with the Discrete Time Fast Fourier Transform at the source point.

The dispersion diagram shows that the shear-Alfven wave in  $L=1.4286$  has its velocity ranging from  $0.4175 \times 10^{-8}$  to  $1.3395 \times 10^{-8}$  m/s. This can be verified by calculating the theoretical Alfven Wave Velocity along  $L=1.4286$  from Equation 3.1.

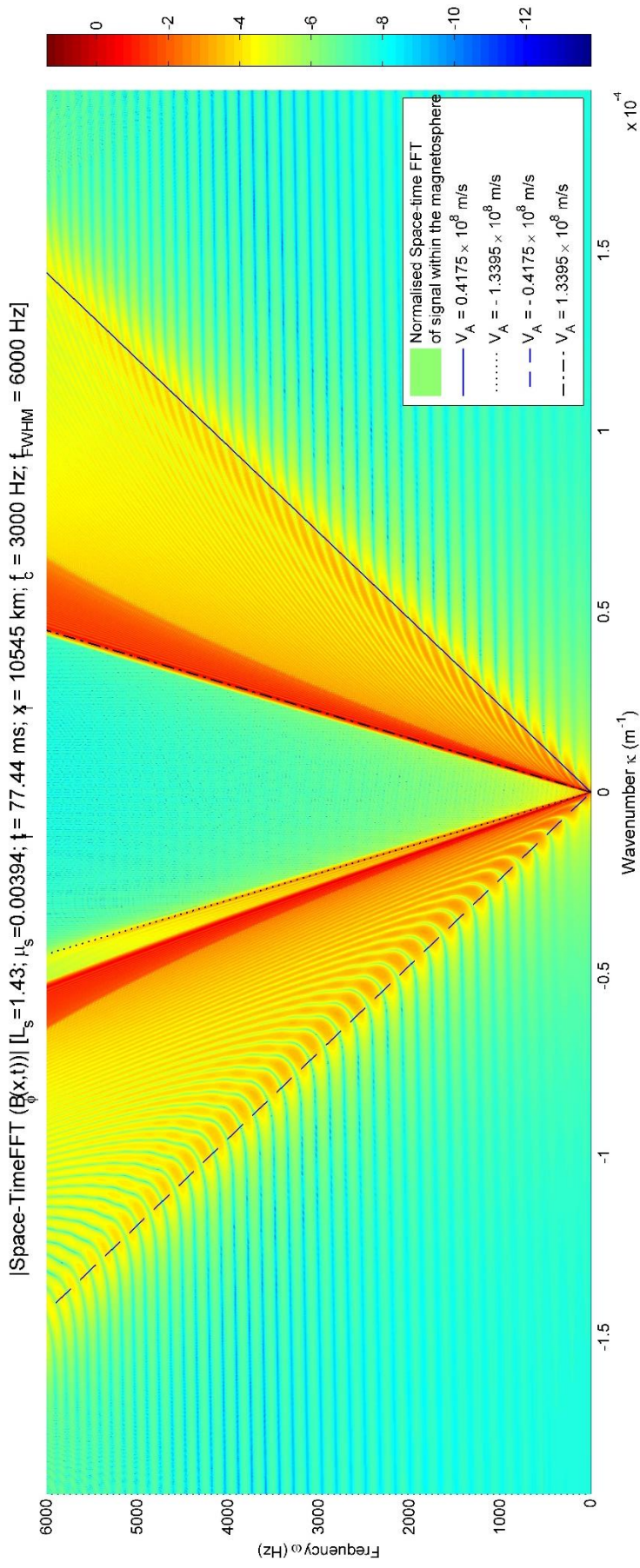


Figure 3.13: Dispersion diagram of a Shear-Alfven Wave propagating in  $L=1.43$ .

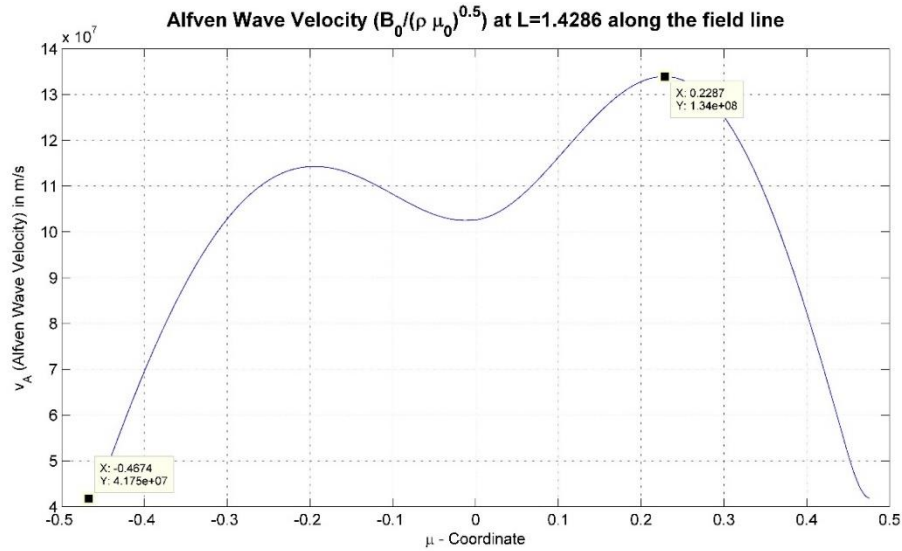


Figure 3.14: Alfven Wave Velocity in m/s along L=1.43

Figure 3.14 shows the variation of theoretical Alfven Wave velocity along L=1.43. From Figure 3.14, one can see that the velocity of the wave in the Dispersion Diagram lies between the maximum and minimum Alfven wave velocities calculated along L=1.4286.

### 3.3.3. Randomizing the Phase-spectrum of the Shear-Alfven Wave

Consider a case where the Gaussian shear-Alfven wave source (with bandwidth 6000Hz and centred at 3000Hz) is generated at one of the boundaries and allowed to propagate for 0.038 seconds (enough to cover the entire length till the next boundary). Figure 3.15 and 3.16 shows the Amplitude and Phase spectrum respectively of such a shear-Alfven Wave. The phase spectrum represented in Figure 3.16, shows the constant phase lines, whose slope describes the phase velocity of the Alfven wave.

Figure 3.17, is the randomized phase spectrum generated by the random number generator function, RAND in MATLAB. This randomized phase, when multiplied with the Amplitude of the Alfven wave in wavenumber-frequency domain, and operated on by Inverse Discrete Fast Fourier Transform will produce a space-time signal which is equivalent to simple random noise as shown in Figure 3.18. The random noise will however retain the amplitude spectrum of a shear-Alfven wave in the particular L-shell.

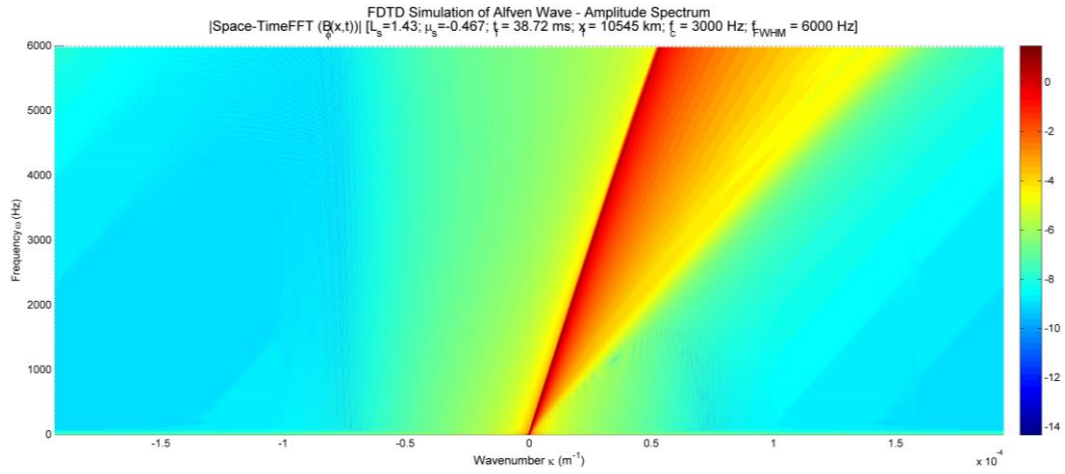


Figure 3.15: Amplitude Spectrum of the  $B_\phi$  field of an Alfvén Wave along  $L=1.4286$ .

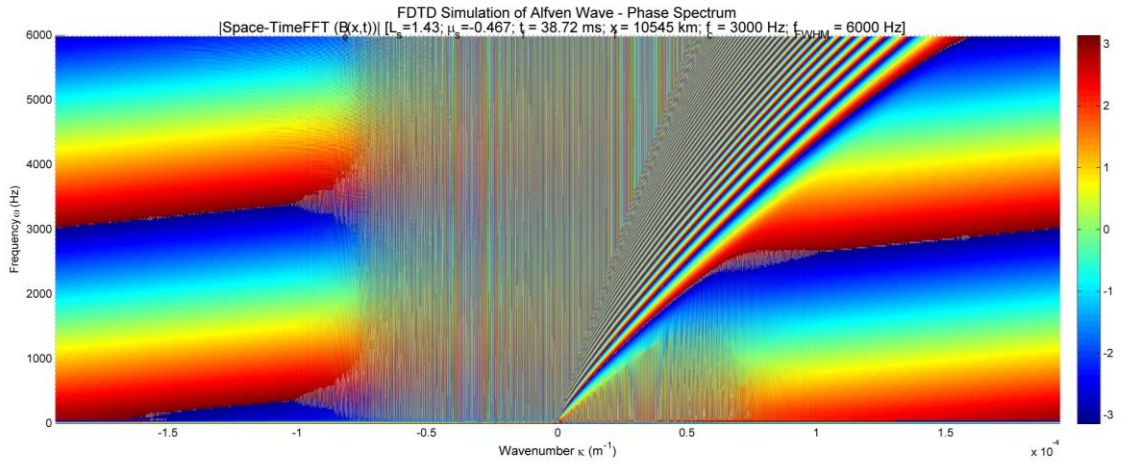


Figure 3.16: Phase Spectrum of the  $B_\phi$  field of an Alfvén Wave along  $L=1.4286$ .

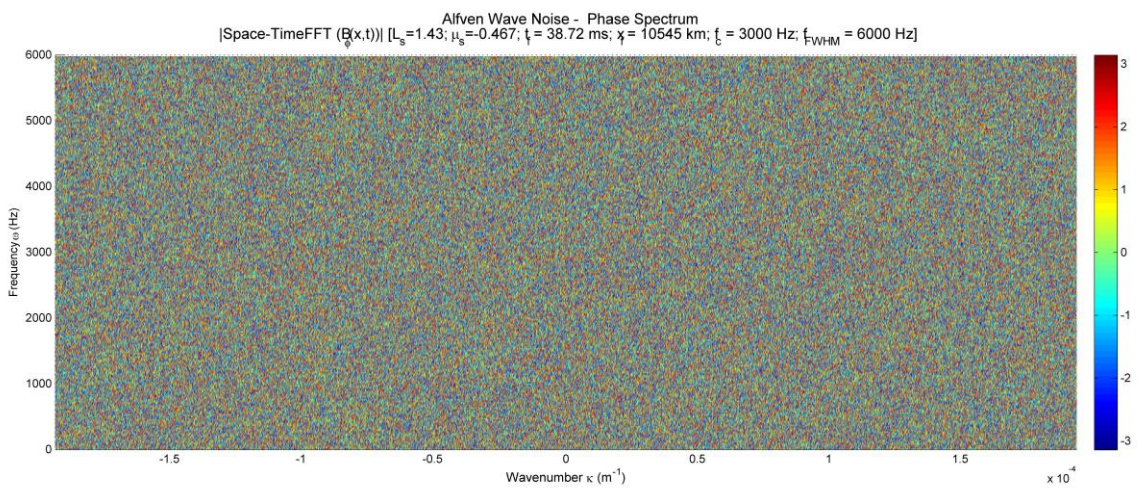


Figure 3.17: Randomized Phase Spectrum of the  $B_\phi$  field generated by random number generator.

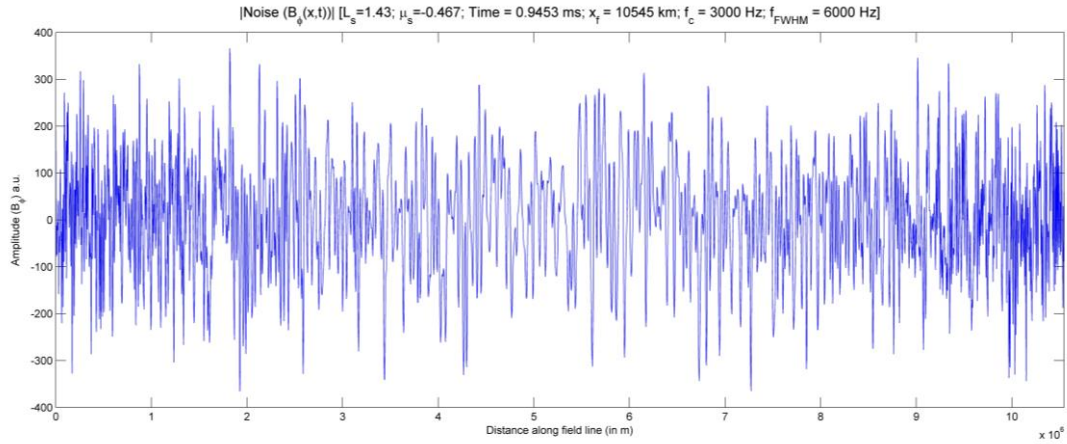


Figure 3.18:  $B_\phi$  ( $t=0.94$  ms) noise of 6000 Hz bandwidth along space.

A Discrete Space-Time FFT of Figure 3.18 will return back exactly an amplitude and phase spectrum as seen in Figure 3.15 and 3.16. The result of this section of the simulation is therefore Shear-Alfven Wave noise in the desired L-shell.

### 3.4. 3-D Trajectory Solver for Charged Particles in the Radiation Belts

This module implements the 4<sup>th</sup> order Runge-kutta method using the ODE45 function in MATLAB to solve the Newton-Lorentz force equation and determine the trajectory of a charged particle in the Earth's Dipole magnetic field.

Recall the Newton-Lorentz force equation:

$$\frac{d(\gamma m \mathbf{v})}{dt} = q\mathbf{E}(\mathbf{r}) + q \mathbf{v} \times \mathbf{B}(\mathbf{r}) \dots \mathbf{Eq. 2.9}$$

Here  $\gamma = \left(1 - \frac{v^2}{c^2}\right)^{-\frac{1}{2}}$  is the relativistic factor and  $\mathbf{v}$  is the particle speed.

The magnetic dipole field of the Earth is modelled by the following equation presented in Section 2.2.1:

$$B_{dip} = -\frac{B_0 R_E^3}{r^5} [3xz\hat{\mathbf{e}}_x + 3yz\hat{\mathbf{e}}_y + (2z^2 - x^2 - y^2)\hat{\mathbf{e}}_z] \dots \mathbf{Eq. 2.10}$$

Where  $B_0 = 3.07 \times 10^{-5} T$ ,  $R_E = 6.3712 \times 10^6 m$

The trajectory solver is capable of incorporating time-varying electric and magnetic fields in the Newton-Lorentz force equation. Apart from the particle's trajectory, it can also generate the

trajectory of the gyrocentre (See Figure 3.19), gyro-radii, gyro-frequency along the trajectory of the particle and the equatorial pitch angle at the locations where the particle crosses the equatorial plane.

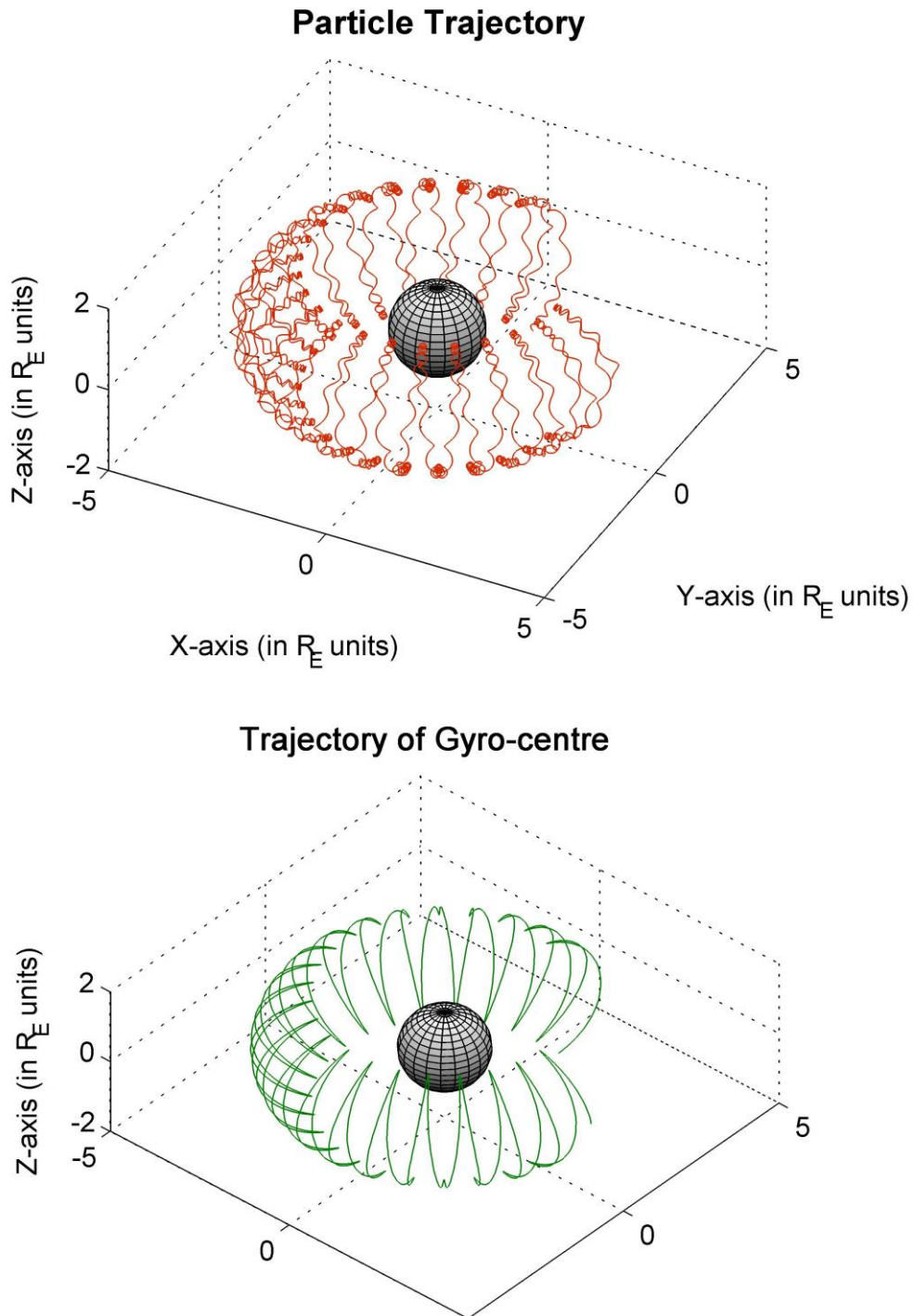


Figure 3.19: The trajectory and the gyrocentre path of a 15 MeV proton in L-shell = 4 generated by the simulation module.

### 3.5. Incorporation of 3-D Alfvén Wave noise into the 3-D Trajectory Solver

The space-time varying Alfvén wave noise fields (both  $B_\phi^{noise}$  and  $E_v^{noise}$ ) are generated from the dispersion diagrams presented in Section 3.3, **by enforcing an upper frequency limit of 100 Hz** (as ion cyclotron frequency  $f_{ci} \sim 200 \text{ Hz}$  at  $L=1.4286$ ). The  $B_\phi^{noise}$  field is then normalized with  $B_{\phi,rms}^{noise} = \frac{\int (B_\phi^{noise}(t))^2 dt}{\int dt}$  and multiplied by  $B_{wave} = \sqrt{2\mu_0 P}$ , where  $P$  is the wave power. This ensures that power of the Alfvén wave noise is specified by the wave power value  $P$  in watts.  $E_v$  is then calculated as  $E_v^{noise}(s) = v_A(s) \times B_\phi^{noise}(s)$ . Both the  $B_\phi^{noise}(s, t)$  and  $E_v^{noise}(s, t)$  are then incorporated into the Newton-Lorentz force equations after the appropriate coordinate transformation.

$$\frac{d(\gamma m \mathbf{v})}{dt} = q \mathbf{E}_{noise}(\mathbf{r}) + q \mathbf{v} \times (\mathbf{B}_{static}(\mathbf{r}) + \mathbf{B}_{noise}(\mathbf{r})) \dots \text{Eq. 3.2}$$

### 3.6. Acquiring the Equatorial Pitch Angle Distribution

Every time the particle's trajectory crosses the equatorial plane, the parallel and perpendicular velocities are recorded to estimate the equatorial pitch angle. By solving the trajectories of a 1000 test particles with an initial pitch angle, the equatorial pitch angle after one-half bounce period is estimated. This gives the scattered equatorial pitch angle distribution due to the shear-Alfvén-wave noise with the specified wave power.

## CHAPTER 4

### 4. RESULTS

#### 4.1. Input Parameters

The simulations described in Section 3 was run with the following input parameters, and the scattered pitch angle distribution was obtained.

Wave Power	:	$P = 6 \times 10^{-9} \text{ watts}$
Wave frequency range	:	0 to 100 Hz
L-shell	:	1.4286
Type of particle	:	<i>Proton</i>
Energy of particle	:	$1 \text{ MeV}$
Time of exposure to noise	:	$1.1 \text{ seconds}$ (~ Half bounce period)
Total number of particles	:	1000
Initial Equatorial Pitch Angle	:	$60^\circ$

Note that the electric field noise was neglected in this particular simulation in order to compare it with the theoretical approximation described in Section 2.3.

#### 4.2. Scattering of Equatorial Pitch Angle Distribution

Figure 4.1 shows both the initial and scattered equatorial pitch angle distribution. As described in Section 3.6, a test particle approach was followed where motion of a single charged particle, in this case a 1 MeV protons, was simulated in the Earth's dipole field with Alfvén wave noise superposed on it. This step was repeated 1000 times, to get a scattered pitch angle distribution for 1000 particles. The equatorial pitch angle, as described in 2.2.2, is a measure of the trajectory of the particle as the Earth's dipole magnetic field is completely described.

Figure 4.2, shows a Gaussian fit on the scattered equatorial pitch angle distribution. The fit gives a standard deviation  $\sigma = 8.70$  for the distribution. From this, the Full Width at Half Maximum ( $FWHM = 2.35 \sigma$ ) of the equatorial pitch angle distribution was acquired:

$$\Delta\alpha_{simulations}^{eq} = 20.44^\circ$$

Using Equation 2.16:  $\Delta V_{\parallel} = \left(\frac{qV_{\perp}B_w}{m}\right)\Delta t$  and Equation 2.15:  $\Delta\alpha = -\frac{\Delta V_{\parallel}}{V_{\perp}}$  the maximum pitch angle scattering due to the magnetic noise produced by the Alfvén wave is:

$$\Delta\alpha_{estimate}^{eq} = 23.90^{\circ}$$

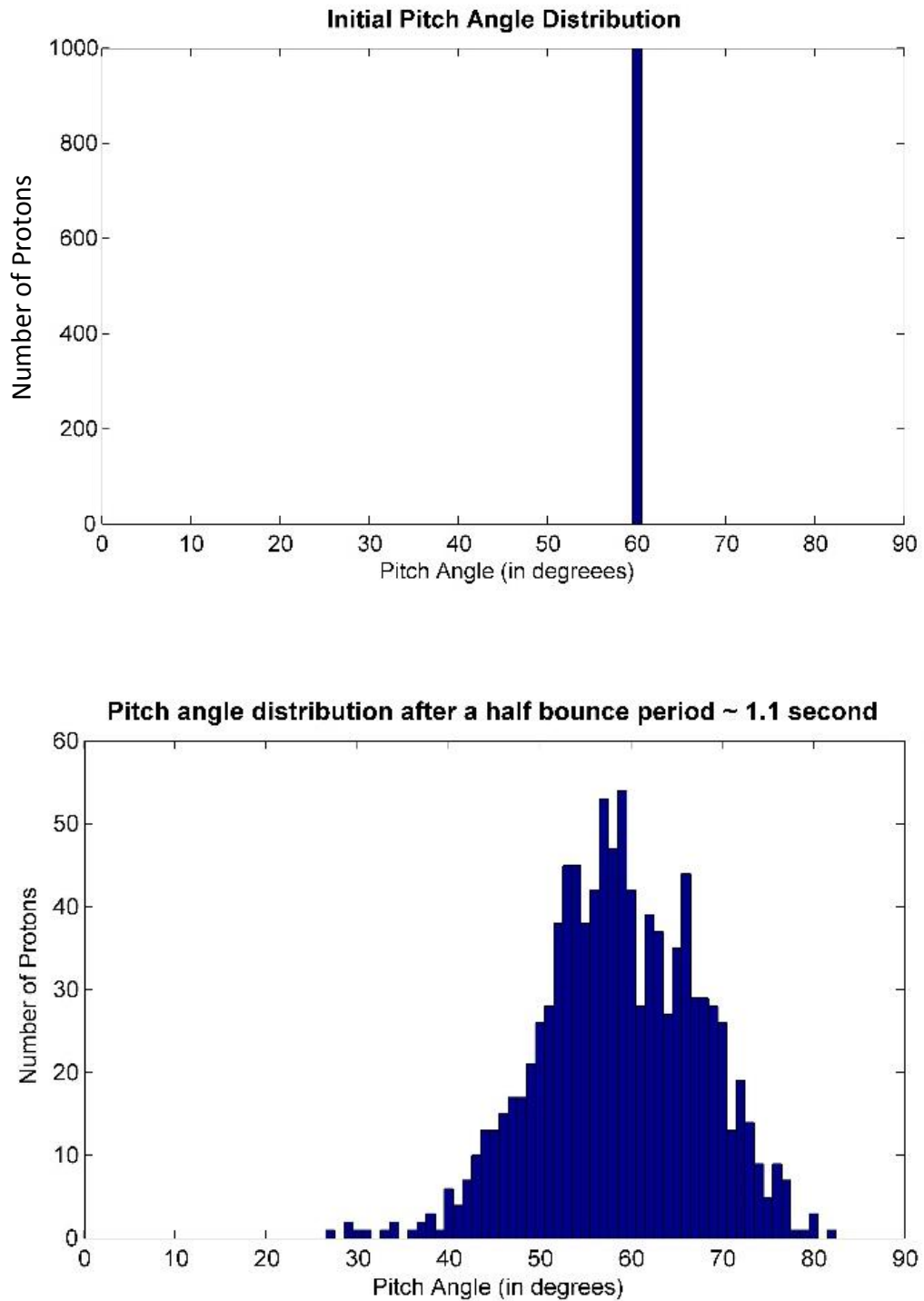


Figure 4.1: Initial (above) and scattered (below) equatorial pitch angle distribution (Total number of protons = 1000)

The scatter in the equatorial pitch angle distribution, is mainly due to the random force that is being exerted on the particle caused due to Alfvén wave noise. This random force causes the  $V_{\parallel}$  and  $V_{\perp}$  of the particles to change, and hence the pitch angle ( $\alpha = \tan^{-1}(V_{\perp}/V_{\parallel})$ ) of the particles also change.

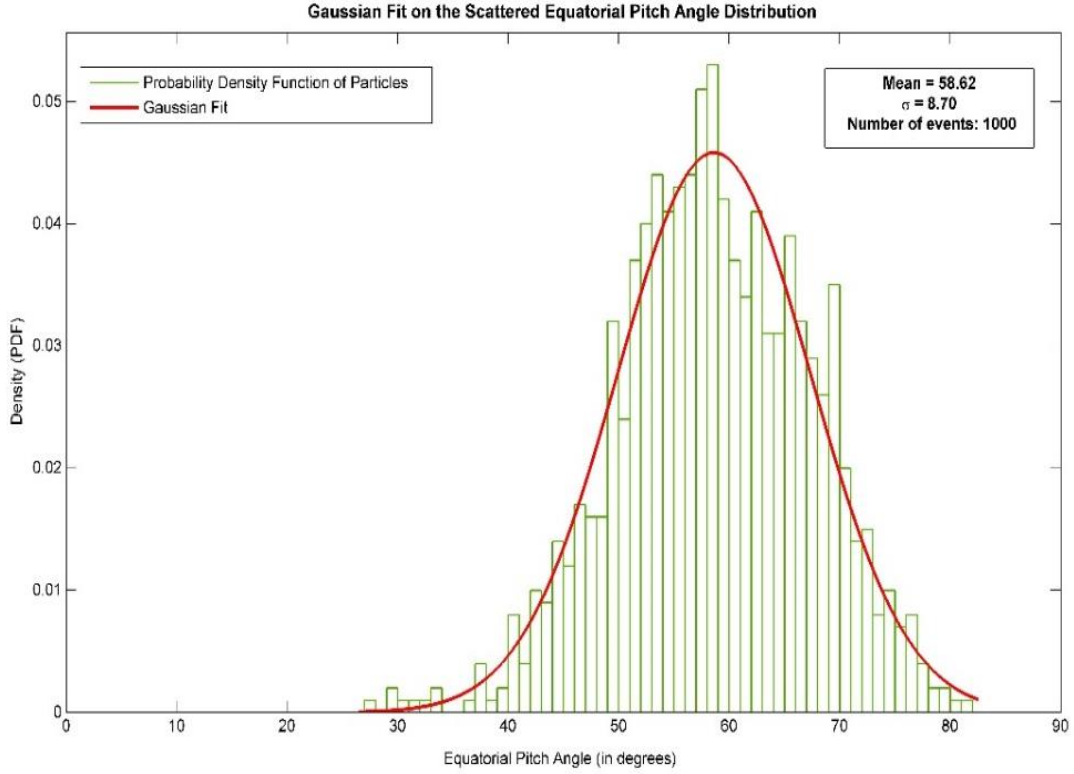


Figure 4.2: Gaussian fit on the scattered equatorial pitch angle distribution

### 4.3. Scattering of Mirror Points

The mirror point location for a charged particle undergoing helical motion in the Earth's dipole field can be calculated directly from the value of the equatorial pitch angle of the particle.

By solving Equation 2.13 mentioned in Section 2.2.3,

$$\sin^2 \alpha_{eq} = \frac{\sin^6 \theta_m}{\sqrt{1 + 3 \cos^2 \theta_m}}$$

we can find the polar angle of the mirror point  $\theta_m$ . With this we can find the mirror point altitude by using the following formulae:

$$r_m = R_E (L \sin^2 \theta_m - 1)$$

Figure 4.3 shows how the particle's mirror points also scatter through the interaction with the Alfvén wave noise. Particles with mirror points below 0 km are lost forever due to collision

with the Earth's surface (these are particles with equatorial pitch angle  $\alpha_{eq}$  less than the loss cone angle  $\alpha_l$ ). Figure 4.4 shows the variation of the mirror point altitude of a particle in the L-shell 1.4286 with equatorial pitch angle. The mirror point altitude of the initial distribution of particles (with the equatorial pitch angle =  $60^\circ$ ) is approximately 2175 km.

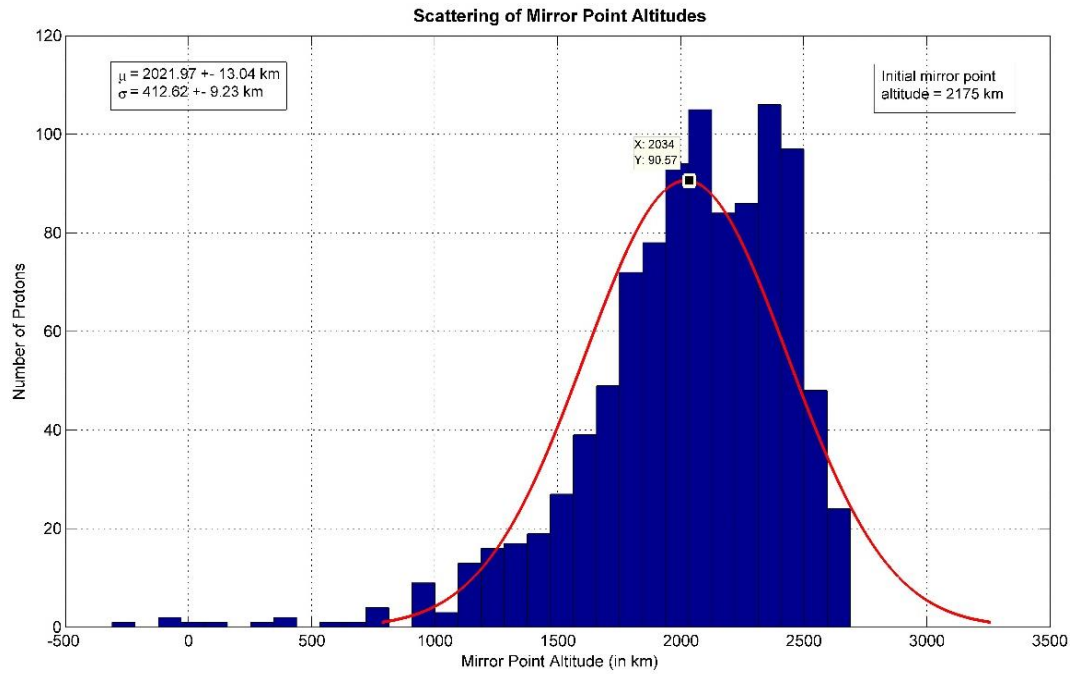


Figure 4.3: Scattering of mirror point altitudes of the particles.

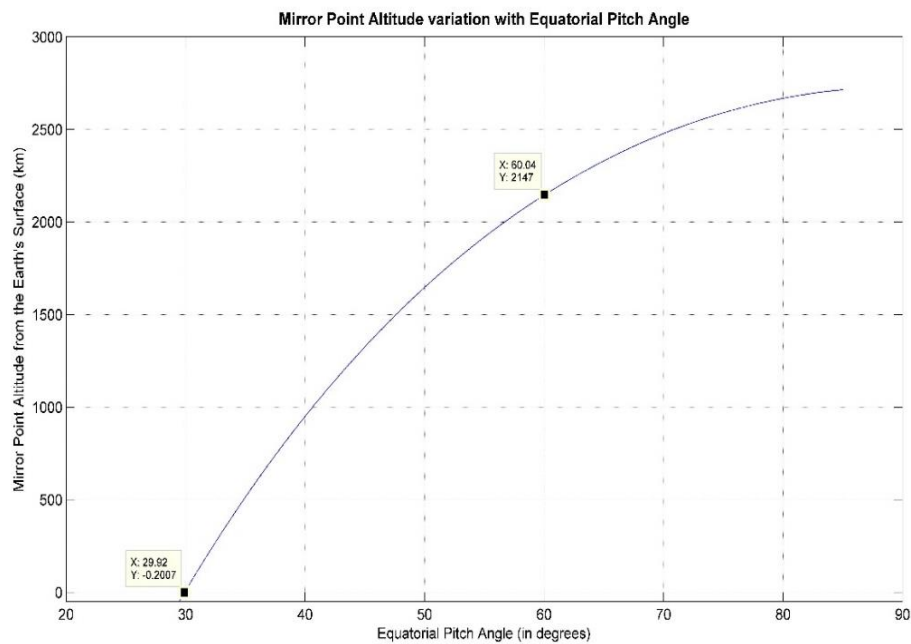


Figure 4.4: Variation of mirror point altitude with equatorial pitch angle.

Note that the loss cone angle for a particle in the L-shell 1.4268 is about  $30^{\circ}$ . This can be verified from Figure 2.2 and Figure 4.4. We can calculate the number of particles with the equatorial pitch angle ( $\alpha_{eq}$ ) less than the loss cone angle ( $\alpha_l$ ) from the scattered equatorial pitch angle and mirror point altitude distributions obtained above.

$\therefore$  The percentage of particles with  $\alpha_{eq}$  less than  $\alpha_l = 0.3\%$ .

The simulation modules described in Section 3 can be used for predicting the scattering of pitch angles and mirror point altitudes for any initial distribution of particles.

## CHAPTER 5

### 5. CONCLUSION

#### 5.1. Summary

In this report, we have presented the 3D FDTD simulations developed in Orthogonal Dipole Coordinates which has been used to estimate the shear-Alfven wave noise in a particular L-shell in the plasmasphere. We have also analysed the effect of the shear-Alfven noise of a specified power on the equatorial pitch angle distribution of charged particles using the Newton-Lorentz force equations. In our study we have focused on the plasma and magnetic field parameters along L=1.4286 field line. This was chosen as it was within the L-shell of interest for the IIT Madras Student Satellite Project being developed for measuring precipitated particles.

The shear-Alfven wave noise is seen to induce scattering of the equatorial pitch angle of the radiation belt particles. An equatorial pitch angle scattering of about  $\text{FWHM} = 20.44^\circ$  was observed due to interaction with of shear-Alfven wave noise and thousand protons of 1 MeV kinetic energy and initial pitch angle of  $60^\circ$ . The pitch angle scattering estimated by the simulation and that predicted by the approximate formulae (Eq. 2.15) are within  $\sim 4^\circ$  of each other. This validates the overall correctness of the simulations and procedures followed. In this case the scattering resulted in 0.3% of the particles being lost from the radiation belts.

#### 5.2. Future Work

The simulation tools developed for the present work are important for further analysis of the physics of wave-particle interaction in the radiation belts. However, in the present report only a single case of initial pitch angle distribution and wave power has been analysed. A parametric study has to be conducted in order to completely understand the behaviour of the particle distribution due to its interaction with shear-Alfven noise. In future, the effect on the pitch angle distribution due to interaction of *coherent* shear-Alfven wave can be studied by making minor modifications to the existing simulation modules.

Furthermore, experimental validation of these simulations can be performed by accessing the data gathered by the recent NASA mission, named the Van-Allen Probes. The mission contains charged particle detectors (Relativistic Proton Spectrometer, RPS; Energetic Particle, Composition and Thermal Plasma Suite, ECT) and several other magnetic field and electric field sensors (Electric Field and Waves Suite, EFW; Electric and Magnetic Field Instrument Suite and Integrated Science, EMFISIS). The electric field and magnetic field data can be used to estimate the precipitation of particles in a particular L-shell, and then verified with flux changes observed in the data gathered by the charge particle detectors.

## REFERENCES

- [1] M. Walt, Introduction to geomagnetically trapped radiation, Cambridge University, 1994.
- [2] L. R. Lyons, R. M. Thorne and C. F. Kennel, "Electron pitch-angle diffusion driven by oblique whistler mode turbulence," *J. Plasma Phys.*, vol. 6, p. 589, 1971.
- [3] L. R. Lyons, R. M. Thorne and C. F. Kennel, "Pitch-angle diffusion of radiation belt electrons within the plasmasphere," *J. Geophys. Res.*, vol. 77, p. 3455, 1972.
- [4] M. Schulz and L. J. Lanzerotti, Particle Diffusion in the Radiation Belts, New York: Springer, 1973.
- [5] L. R. Lynos, "Comments on pitch-angle diffusion in the radiation belts," *J. Geophys. Res.*, vol. 78, no. 28, pp. 6793-6797, 1973.
- [6] L. R. Lynos, "General relations for particle diffusion in pitch angle and energy," *J. Plasma Phys.*, vol. 12, p. 45, 1974.
- [7] L. R. Lynos, "Pitch angle and energy diffusion coefficients from resonant interactions with ion-cyclotron and whistler waves.," *J. Plasma Phys.*, vol. 12, p. 417, 1974.
- [8] C. S. Roberts, "Electron loss from the Van Allen zones due to pitch angle scattering by electromagnetic disturbances," in *Radiation Trapped in the Earth's Magnetic Field*, New Jersey, Springer Netherlands, 1966, pp. 403-421.
- [9] R. L. Lysak, "Magnetosphere-ionosphere coupling by Alfvén waves at midlatitudes," *Journal of Geophysical Research*, vol. 109, p. A07201, 2004.
- [10] J. A. Proehl, W. Lotko, I. Kouznetsov and S. D. Geimer, "Ultralow-frequency magnetohydrodynamics in boundary-constrained geomagnetic flux coordinates," *Journal of Geophysical Research*, vol. 107, no. A9, p. 1225, 2002.
- [11] C. Uberoi, Earth's Proximal Space, Hyderabad: Universities Press (India) Limited, 2000.
- [12] U. S. Inan, "Non-Linear Gyroresonant Interactions of Energetic Particles and Coherent VLF Waves in the Magnetosphere," Stanford University, Stanford, California, 1977.

- [13] "SPENVIS, The Space Environment Information System," European Space Agency, 1997-2012. [Online]. Available: <http://www.spennis.oma.be/help/background/traprad/motion.gif>. [Accessed 12 06 2013].
- [14] P. M. Bellan, *Fundamentals of Plasma Physics*, New York: Cambridge University Press, 2006.
- [15] R. Fitzpatrick, *Plasma Physics*, Austin, 2011.
- [16] B. T. Tsurutani and G. S. Lakhina, "Some Basic Concepts of Wave-Particle Interactions in Collisionless Plasmas," *Reviews of Geophysics*, pp. 491-502, November 1997.
- [17] "Matlab Central File Exchange," Mathworks, [Online]. Available: [http://www.mathworks.in/matlabcentral/filechange/34388\\_international\\_geomagnetic\\_reference\\_field\\_igrf\\_model](http://www.mathworks.in/matlabcentral/filechange/34388_international_geomagnetic_reference_field_igrf_model). [Accessed 26 Jan 2013].
- [18] G. D. L., "Space Plasma Physics, Plasmaspheric Models," NASA, 19 June 2009. [Online]. Available: <http://plasmisphere.nasa.gov/models/>. [Accessed 24 01 2013].

## APPENDIX 1: Simulation Codes

### 6.1. 3-D FDTD Simulations in Orthogonal Dipole Coordinate System

This simulation module consists of the following MATLAB script files and functions:

1. `main.m` : This is the main script file, that calculates the shear-Alfvén wave noise, if the specific magnetic field line and plasma parameters are given. Specific input file : `e_dat.mat` is required to input the electron densities. The output is in the form of “`calculate_fft.mat`”.
2. `calculateh.m()` : This is a function that takes in the  $\nu$  and  $\mu$  spatial coordinate arrays with the size of the  $\phi$  array and  $R_E$  value. It calculates the scale factors for the Dipole Coordinate System. Returns a 3-D matrix of scale factors with values at every spatial location in the simulations.
3. `calculateh1()` : This is a function that takes in the  $\nu$  and  $\mu$  spatial coordinate arrays and  $R_E$  value. It calculates the scale factors for the Dipole Coordinate System. Returns a 2-D matrix of scale factors with values at every spatial location in the simulations at arbitrary  $\phi$ .
4. `plot_mer()` : Plots the distribution of the required electric or magnetic field in the meridional Plane of the dipole coordinate system.
5. `plot_equ()` : Plots the distribution of the required electric or magnetic field in the equatorial plane of the dipole coordinate system.
6. `plot_fft_a()` : Plots the Dispersion Diagram using values from `calculate_fft.mat`

This matlab script was made and run in MATLABr2012a in the VIRGO supercluster at IIT Madras. Note that `main.m` needs access to `igrf.m` and the set of functions required to extract magnetic field data from the IGRF model. Please see the ref: [17] to download the `igrf()` module compatible with MATLAB.

### 6.1.1. main.m

```
%% 3D-FDTD Implementation for Generating Alfven Wave Noise
% InOrthogonal Dipole Coordinates
% Uses the following:
% Global Core Plasma Model Version 2.4
% IGRF Model MATLAB (Year ?)
%
%
% Program By Nithin Sivadas, AE08B014
% Guide : Prof. Harishankar Ramachandran
%       : Dr. T. M. Muruganandam
%
% Last Updated on : 12th June 2013

%%
clc;
clear all; close all;
tic;

%% Important Variables

% Mass of electron
me = 9.10938188*10^-31;

% Importing Electron Density created from Fortran Code that
extract
% plasma parameters from GCPM Ver. 2.4
e_den=importdata('e_den.mat');

% Time defined for IGRF Model
time = datenum([2002 7 17 6 30 0]);

% Number of iterations (for entire simulation)
time_tot=16384*16;

% Defining the wavelength of the source
frequency=3000; % in Hz

%% Defining the Simulation space

% Extent of radiation belts
% Spatial grid step length

dn=-0.01;
dm=2.3026e-04;
dp=2*pi/4;

% Size of the grid
Li=0.8;
Lf=10;
Ls=1.4286;
Sn=-1/Ls+1*dn;
Sn1=-1/Ls-1*dn;
Sm=0.4755;
Sm1=-0.4674;
Sp=0;
Sp1=2*pi;
```

```

mu(1)=Sm1;
Nm=round((Sm-Sm1)/dm)+1;
for i=2:1:Nm
    mu(i)=mu(i-1)+dm;
end;
nu=Sn1:dn:Sn;
phi=Sp:dp:Sp1;

% Number of cells along the n and m directions
Nn=size(nu);
Nn=Nn(2);
Nm=size(mu);
Nm=Nm(2);
Np=size(phi);
Np=Np(2);

%%
% Defining the speed of light
c=3e+8;

%%
% Defining source locations and distribution

nsource = 2;
msource = 2;
psource = round(Np/2);

%% Scale factors and coordinate transformation
RE=6371.2*10^3;

[hn_0_0, hp_0_0, hm_0_0]=calculateh(nu,mu,Np,RE);
[hn_1_1, hp_1_1,
hm_1_1]=calculateh(nu+(0.5*dn)*ones(1,Nn),mu+(0.5*dm)*ones(1,Nm),Np,RE);
[hn_0_1, hp_0_1,
hm_0_1]=calculateh(nu,mu+(0.5*dm)*ones(1,Nm),Np,RE);
[hn_1_0, hp_1_0,
hm_1_0]=calculateh(nu+(0.5*dn)*ones(1,Nn),mu,Np,RE);

alpha=(256/27)*(mu'.^2)*(nu.^-4);
beta=(1+(1+alpha).^0.5).^2/3;
gamma=(alpha).^(1/3);
k=0.5*((beta.^2+beta.*gamma+gamma.^2)./(beta)).^1.5;
r=- (4*k./((1+k).*(1+(2*k-1).^0.5)))*(diag(RE*(nu.^-1)));
costheta=(RE^-2)*diag(mu)*(r.^2);
sintheta=(1-costheta.^2).^0.5;
r1=r;
costheta1=costheta;
sintheta1=sintheta;

for i=1:1:Np-1
    r=cat(3,r,r1);
    costheta=cat(3,costheta,costheta1);
    sintheta=cat(3,sintheta,sintheta1);
end
cosphi=cos(phi);
sinphi=sin(phi);

for j=1:1:Nn-1

```

```

        cosphi=cat(1,cosphi,cos(phi));
        sinphi=cat(1,sinphi,sin(phi));
end;

%% Calculating the B-field from IGRF Model
% Converting the Geomagnetic coordinates to Geocentric

theta_geo_centric=zeros(Nn,Nm,Np);
phi_geo_centric=zeros(Nn,Nm,Np);
Bx=zeros(Nn,Nm,Np);
By=zeros(Nn,Nm,Np);
Bz=zeros(Nn,Nm,Np);
theta_pole=11.018*pi/180;
phi_pole=289.095*pi/180;

p=1;
for i=1:1:Nn
    for j=1:1:Nm
        theta_geo_centric(j,i,p)=acos(cos(theta_pole)*cos(theta_l(j,i)
+ sin(theta_pole)*sin(theta_l(j,i)*cos(2*pi-phi(p)));
        if
            costheta_l(j,i)<cos(theta_pole)*cos(theta_geo_centric(i,j,p))
                disp([' Percentage Complete IGRF Model']);
                phi_geo_centric(j,i,p)=phi_pole+pi-
                asin(sin(theta_l(j,i)*sin(phi(p)))/sin(theta_geo_centric(j,i,p)));
            else

phi_geo_centric(j,i,p)=phi_pole+asin(sin(theta_l(j,i)*sin(phi(p)))/sin(t
heta_geo_centric(j,i,p)));
            end;
            [Bx(i,j,p), By(i,j,p), Bz(i,j,p)]=igrf(time,(0.5*pi-
theta_geo_centric(j,i,p))*180/pi,(phi_geo_centric(j,i,p))*180/pi,(r(j
,i,p))*0.001,'geocentric');
            clc;
            completel=100*(j/Nm);
            disp([' Percentage Complete for 1 Nn= ' num2str(completel,
' %g') ' %']);

            end;
            clc;
            completel=100*(i/Nn);
            disp([' Percentage Complete IGRF Model= ' num2str(completel,
' %g') ' %']);
            end;

for p=2:1:Np
    Bx(:,:,p)=Bx(:,:,1);
    By(:,:,p)=By(:,:,1);
    Bz(:,:,p)=Bz(:,:,1);
end;
B0=((Bx.^2+By.^2+Bz.^2).^0.5)*10^-9;

%% Defning the permittivity & permeability distribution (air)
A=ones(Nn,Nm,Np);
A=(e_den')*(me)*10^6;
for i=1:1:Np
    A(:,:,i)=(e_den')*(me)*10^6; % As electron density is
number of electrons/cm3
end;

```

```

mu0 = 4*pi*1e-7;
epsilon0 = (1/(36*pi))*1e-9;
E_den=A; % Density of electrons in Kg/m^3
A=1+(c.^2)*mu0*E_den.*((B0).^2);
epsilon=A*epsilon0;

%% Defining Alfven Wave velocity
V1=(epsilon*mu0).^-1;
% V1=(ones(Nn,Nm,Np))* (1.339e+08).^2;
V1(isnan(V1))=(3*10^8)^2;

[MU, NU, PH] = meshgrid(mu,nu,phi);

%% Courant Stability Factor
S=1/(3^(0.5));
% S=0.5;
% contour(r.*sintheta,r.*costheta,MU',Nm,'black');
% hold on;
% contour(r.*sintheta,r.*costheta,NU',Nn,'blue');

%% Initialization of the field matrices
Bn=zeros(Nn,Nm,Np);
Bm=zeros(Nn,Nm,Np);
Bp=zeros(Nn,Nm,Np);
En=zeros(Nn,Nm,Np);
Em=zeros(Nn,Nm,Np);
Ep=zeros(Nn,Nm,Np);

%% Temporal grid step obtained
V=c;

deltat=S*(min(min(min(abs(hn_0_0(:, :, psource).*dn))), (min(min(abs(h
m_0_0(:, :, psource).*dm)))))/V;
deltat=min(deltat,S*(min(min(abs(hp_0_0(:, :, psource).*dp))))/V);

%% Defining the variation of conductivities at the boundary for PML
% Right now it is set to inactive, as the Ionosphere B.C. is made to
% be perfectly reflective.
sigma=0*ones(Nn,Nm,Np);
PML=round((-1/5)-Sn1)./dn);%PML Boundary

% PML_a=10;
% PML_tn=size((Sn1:dn:-1/5)');
% PML_tn2=size((-1/1.02:dn:Sn)');
% PML_fn=(PML_a)*(1*(PML_tn(1):-1:1)).^3;
% PML_fn2=(PML_a)*(1*(PML_tn2(1)+1:-1:1)).^3;
% PML_tm=size((Sm1:dm:Sm1+20*dm)');
% PML_tm2=size((Sm-20*dm:dm:Sm)');
% PML_fm=(PML_a)*(1*(PML_tm(1):-1:1)).^3;
% PML_fm2=(PML_a)*(1*(PML_tm(1):-1:1)).^3;
%
% for i=1:1:Nm
%     for j=1:1:Np
%         sigma(1:1:PML_tn(1),i,j)=(PML_fn);
%         sigma(Nn:-1:Nn-PML_tn2(1),i,j)=PML_fn2;
%     end;

```

```

% end;
%
% for i=1:1:Nn
%     for j=1:1:Np
%         sigma(i,1:1:PML_tm(1),j)=sigma(i,1:1:PML_tm(1),j)+PML_fm;
%         sigma(i,Nm:-1:Nm-PML_tm2(1)+1,j)=sigma(i,Nm:-1:Nm-
PML_tm2(1)+1,j)+PML_fm2;
%     end;
% end;

sigma_star=sigma.*mu0;

%% Gaussian Source Parameters
Fw=6000; % Bandwidth of the signal
Ft=(2*log(2))/(pi*Fw);
norm=((2*(log(2))^0.5)/(Ft*pi^0.5))^0.5;
t0=4*Ft;

figure20=figure('visible','off');
axes20 = axes('Parent',figure20);

%% Update loop
for u=1:1:time_tot
    u1=1;
    u2=Nn-1;
    u11=1;
    u21=Nm-1;
    k1=1;
    k2=Np-1;

    %Vector update for 3D-FDTD

    Bn(u1:u2,u11+1:u21+1,k1+1:k2+1)=((1-
deltat.*sigma_star(u1:u2,u11+1:u21+1,k1+1:k2+1)./(2*mu0))./(1+deltat.
*sigma_star(u1:u2,u11+1:u21+1,k1+1:k2+1)./(2*mu0))).*Bn(u1:u2,u11+1:u
21+1,k1+1:k2+1)-
(deltat./((hp_0_1(u1:u2,u11+1:u21+1,k1+1:k2+1).*hm_0_1(u1:u2,u11+1:u2
1+1,k1+1:k2+1)).*(1+deltat.*sigma_star(u1:u2,u11+1:u21+1,k1+1:k2+1)./(
2*mu0))))).*(dp.^-
1).* (hm_0_1(u1:u2,u11+1:u21+1,k1+1:k2+1).*Em(u1:u2,u11+1:u21+1,k1+1:k
2+1)-hm_0_1(u1:u2,u11+1:u21+1,k1:k2).*Em(u1:u2,u11+1:u21+1,k1:k2))-
(dm.^-
1).* (hp_0_0(u1:u2,u11+1:u21+1,k1+1:k2+1).*Ep(u1:u2,u11+1:u21+1,k1+1:k
2+1)-hp_0_0(u1:u2,u11+1:u21+1,k1+1:k2+1).*Ep(u1:u2,u11+1:u21+1,k1+1:k2+1)));
    Bp(u1+1:u2+1,u11+1:u21+1,k1:k2)=((1-
deltat.*sigma_star(u1+1:u2+1,u11+1:u21+1,k1:k2)./(2*mu0))./(1+deltat.
*sigma_star(u1+1:u2+1,u11+1:u21+1,k1:k2)./(2*mu0))).*Bp(u1+1:u2+1,u11
+1:u21+1,k1:k2)-
(deltat./((hm_1_1(u1+1:u2+1,u11+1:u21+1,k1:k2).*hn_1_1(u1+1:u2+1,u11+
1:u21+1,k1:k2)).*(1+deltat.*sigma_star(u1+1:u2+1,u11+1:u21+1,k1:k2)./(
2*mu0))))).*(dm.^-
1).* (hn_1_0(u1+1:u2+1,u11+1:u21+1,k1:k2).*En(u1+1:u2+1,u11+1:u21+1,k1
:k2)-hn_1_0(u1+1:u2+1,u11+1:u21+1,k1:k2).*En(u1+1:u2+1,u11+1:u21+1,k1
:k2))-
(dn.^-
1).* (hm_0_1(u1+1:u2+1,u11+1:u21+1,k1:k2).*Em(u1+1:u2+1,u11+1:u21+1,k1
:k2)-hm_0_1(u1:u2,u11+1:u21+1,k1:k2).*Em(u1:u2,u11+1:u21+1,k1:k2)));
    Bm(u1+1:u2+1,u11+1:u21+1,k1+1:k2+1)=((1-
deltat.*sigma_star(u1+1:u2+1,u11+1:u21+1,k1+1:k2+1)./(2*mu0))./(1+deltat.
*sigma_star(u1+1:u2+1,u11+1:u21+1,k1+1:k2+1)./(2*mu0))).*Bm(u1+1:u2+1,u11
+1:u21+1,k1+1:k2+1)-

```

```

(deltat./((hn_1_0(u1+1:u2+1,u11:u21,k1+1:k2+1).*hp_1_0(u1+1:u2+1,u11:
u21,k1+1:k2+1)).*(1+deltat.*sigma_star(u1+1:u2+1,u11:u21,k1+1:k2+1))./(
2*mu0))))).*(dn.^-
1).* (hp_0_0(u1+1:u2+1,u11:u21,k1+1:k2+1).*Ep(u1+1:u2+1,u11:u21,k1+1:k
2+1)-hp_0_0(u1:u2,u11:u21,k1+1:k2+1).*Ep(u1:u2,u11:u21,k1+1:k2+1))-
(dp.^-
1).* (hn_1_0(u1+1:u2+1,u11:u21,k1+1:k2+1).*En(u1+1:u2+1,u11:u21,k1+1:k
2+1)-hn_1_0(u1+1:u2+1,u11:u21,k1:k2).*En(u1+1:u2+1,u11:u21,k1:k2)));

En(u1+1:u2+1,u11:u21,k1:k2)=((1-
deltat.*sigma(u1+1:u2+1,u11:u21,k1:k2).*0.5))./(1+deltat.*sigma(u1+1:u
2+1,u11:u21,k1:k2).*0.5)).*En(u1+1:u2+1,u11:u21,k1:k2)+(((deltat.*(V1
(u1+1:u2+1,u11:u21,k1:k2)))./(hp_1_0(u1+1:u2+1,u11:u21,k1:k2).*hm_1_0
(u1+1:u2+1,u11:u21,k1:k2)).*(1+deltat.*sigma(u1+1:u2+1,u11:u21,k1:k2)
*0.5))))).*(dp.^-
1).* (hm_1_0(u1+1:u2+1,u11:u21,k1+1:k2+1).*Bm(u1+1:u2+1,u11:u21,k1+1:k
2+1)-hm_1_0(u1+1:u2+1,u11:u21,k1:k2).*Bm(u1+1:u2+1,u11:u21,k1:k2))-
(dm.^-
1).* (hp_1_1(u1+1:u2+1,u11+1:u21+1,k1:k2).*Bp(u1+1:u2+1,u11+1:u21+1,k1
:k2)-hp_1_1(u1+1:u2+1,u11:u21,k1:k2).*Bp(u1+1:u2+1,u11:u21,k1:k2)));
Ep(u1:u2,u11:u21,k1+1:k2+1)=((1-
deltat.*sigma(u1:u2,u11:u21,k1+1:k2+1).*0.5))./(1+deltat.*sigma(u1:u2,
u11:u21,k1+1:k2+1).*0.5)).*Ep(u1:u2,u11:u21,k1+1:k2+1)+(((deltat.*(V1
(u1:u2,u11:u21,k1+1:k2+1)))./(hn_0_0(u1:u2,u11:u21,k1+1:k2+1).*hm_0_0
(u1:u2,u11:u21,k1+1:k2+1)).*(1+deltat.*sigma(u1:u2,u11:u21,k1+1:k2+1)
*0.5))))).*(dm.^-
1).* (hn_0_1(u1:u2,u11+1:u21+1,k1+1:k2+1).*Bn(u1:u2,u11+1:u21+1,k1+1:k
2+1)-hn_0_1(u1:u2,u11:u21,k1+1:k2+1).*Bn(u1:u2,u11:u21,k1+1:k2+1))-
(dn.^-
1).* (hm_1_0(u1+1:u2+1,u11:u21,k1+1:k2+1).*Bm(u1+1:u2+1,u11:u21,k1+1:k
2+1)-hm_1_0(u1:u2,u11:u21,k1+1:k2+1).*Bm(u1:u2,u11:u21,k1+1:k2+1)));

% Source Definition
source = 10^-8*exp(1i*2*pi*frequency*deltat*u)*norm*exp(-
((2*log(2)*(t0-u*deltat)^2)/(Ft^2.0)));

Bp(nsource,msource,:)=Bp(nsource,msource,:)+source;
DFT1(1,u)=source;
DFT2(u,:)=Bp(nsource,:,psource);
EDFT1(1,u)=En(nsource,msource,psource);
EDFT2(u,:)=En(nsource,:,psource);

%Perfect reflecting boundary condition along mu
Bn(:,1,:)=0;
Bn(:,Nm,:)=0;
Bm(:,1,:)=0;
Bm(:,Nm,:)=0;
Bp(:,1,:)=0;
Bp(:,Nm,:)=0;
En(:,1,:)=0;
En(:,Nm,:)=0;
Ep(:,1,:)=0;
Ep(:,Nm,:)=0;

clc;
complete=100*(u/time_tot);
disp([' Percentage Complete = ' num2str(complete, '%g')]);

end;

```

```

%% Defining the number of space and time samples
NFFT=2^nextpow2(time_tot);
k=size(mu);
space_tot=k(2);
SFFT=2^nextpow2(space_tot);

%% Making the space-samples uniform
% Converting from \mu coordinates to s coordinate
DFT3=zeros(time_tot,space_tot);
EDFT3=zeros(time_tot,space_tot);
mus=zeros(1,space_tot);
[hn, hp, hm]=calculateh1(nu,mu,RE);

for i=1:1:k(2)-1
    mus(i+1)=mus(i)+dm*hm(nsource,i);
end;
xx=linspace(0,max(mus),space_tot);

for j=1:time_tot
    DFT3(j,:)=spline(mus,real(DFT2(j,1:1:Nm)),xx);
    DFT3(j,:)=DFT3(j,:).*hamming(space_tot,'periodic');
    EDFT3(j,:)=spline(mus,real(EDFT2(j,1:1:Nm)),xx);
    EDFT3(j,:)=EDFT3(j,:).*hamming(space_tot,'periodic');
end;
dmus=(max(mus)-0)/(space_tot-1);
DFT1(1,:)=DFT1(1,:).*hamming(time_tot,'periodic');
EDFT1(1,:)=EDFT1(1,:).*hamming(time_tot,'periodic');
for j=1:space_tot
    DFT3(:,j)=DFT3(:,j).*hamming(time_tot,'periodic');
    EDFT3(:,j)=EDFT3(:,j).*hamming(time_tot,'periodic');
end;

%% Downsample the frequency as we are only interested in low
frequency
NFFTa=4096;
x=round(time_tot/NFFTa);
time_tot_a=time_tot/x;
deltat_a=deltat*x;
DFT1a=zeros(1,NFFTa);
DFT3a=zeros(NFFTa,SFFT);
DFT2end=DFT2(time_tot,:);
EDFT1a=zeros(1,NFFTa);
EDFT3a=zeros(NFFTa,SFFT);
EDFT2end=EDFT2(time_tot,:);

for i=1:1:SFFT
    for j=1:1:NFFTa
        DFT3a(j,i)=real(mean(DFT3((1+(j-1)*x:1:j*x),i)));
        EDFT3a(j,i)=real(mean(EDFT3((1+(j-1)*x:1:j*x),i)));
    end;
end;

for j=1:1:NFFTa
    DFT1a(j)=real(mean(DFT1(1,(1+(j-1)*x:1:j*x))));
    EDFT1a(j)=real(mean(EDFT1(1,(1+(j-1)*x:1:j*x))));
end;

%% Generating the Dispersion relations through DFFT
c1=((fft((real((DFT3a'))),SFFT)/space_tot)); % FFT(s) of signal
c2=abs(fftshift((fft(c1',NFFTa)/time_tot_a))); % FFT(t) of signal

```

```

p2=(angle(fftshift((fft(c1',NFFTa)/time_tot_a))));
b2=abs(fftshift((fft((real(DFT1a)),NFFTa)/time_tot_a))); % FFT(t) of
source

c1E=(((fft((real((EDFT3a'))),SFFT)/space_tot)); % FFT(s) of signal
c2E=abs(fftshift((fft(c1E',NFFTa)/time_tot_a))); % FFT(t) of signal
p2E=(angle(fftshift((fft(c1E',NFFTa)/time_tot_a))));
b2E=abs(fftshift((fft((real(EDFT1a)),NFFTa)/time_tot_a))); % FFT(t)
of source

% Normalising with the FFT of source
for i=1:SFFT
    c2(:,i)=c2(:,i)./b2';
    c2E(:,i)=c2E(:,i)./b2E';
end;

%% Calculating the Shear-Alfven Wave Noise Signal

a=-pi;
b=pi;
fmax=1000;
f1=1/(deltat_a)/2;
nmax=round(fmax*(NFFTa/2)/f1);
l=size(NFFTa/2-nmax+1:NFFTa/2+nmax);
RandSignal=zeros(NFFTa,SFFT);

    prand=a + (b-a).*rand(l(2),SFFT); %Randomizing the phase
    crand=zeros(NFFTa,SFFT);
    crand(NFFTa/2-nmax+1:NFFTa/2+nmax,1:1:SFFT)=(abs(c2(NFFTa/2-
nmax+1:NFFTa/2+nmax,1:1:SFFT))).*exp(1i*prand);

    for j=1:1:SFFT
        crand(NFFTa/2-nmax+1:NFFTa/2+nmax,j)=crand(NFFTa/2-
nmax+1:NFFTa/2+nmax,j).*tukeywin(l(2)); %tukey window to avoid any
abdrupt jumps in the f-k space
    end;

    % Alfven-wave Noise
    RandSignal(1+(i-
1):1:NFFTa*i,1:1:SFFT)=ifft2(fftshift(crand)*SFFT*NFFTa,NFFTa,SFFT,'n
onsymmetric');

    %f-k dispersion diagram of the noise
fftbrand2=(fftshift(fft2(RandSignal/(SFFT*NFFTa),NFFTa,SFFT)));

%% Saving Data
save('calculate_fft.mat','NFFT','SFFT','deltat','time_tot',
'dmus','mu','nu','mus','msource','nsource','frequency','Fw',
'NFFTa','deltat_a','time_tot_a','c2','p2','DFT1',
'DFT2end','RandSignal','fftbrand2','c2E');

%% Displaying total time taken to run the simulations
disp([' Total CPU Time = ' num2str(toc, '%g')]);

```

### 6.1.2. calculate.m

```
function [ hn3, hp3, hm3 ] = calculateh( nu, mu, Np, RE )
%calculateh
% Calculates the scale factors for the Dipole Coordinate System
% Returns a 3-D matrix of scale factors with values at every
spatial
% location in the simulations.
alpha=(256/27)*(mu'.^2)*(nu.^-4);
beta=(1+(1+alpha).^0.5).^(2/3);
gamma=(alpha).^(1/3);
k=0.5*((beta.^2+beta.*gamma+gamma.^2)./(beta)).^1.5;
r=- (4*k./((1+k).*(1+(2*k-1).^0.5)))*(diag(RE*(nu.^-1)));
costheta=(RE^-2)*diag(mu)*(r.^2);
sintheta=(1-costheta.^2).^0.5;

hn=((r.^2)./(RE*(sintheta).*(1+3*(costheta).^2).^0.5))';
hm=((r.^3)./((RE^2)*(1+3*(costheta).^2).^0.5))';
hp=(r.*sintheta)';

hn3=hn;
hm3=hm;
hp3=hp;
for i=1:1:Np-1
    hn3=cat(3, hn3, hn);
    hm3=cat(3, hm3, hm);
    hp3=cat(3, hp3, hp);
end
```

### 6.1.3. calculateh1.m

```
function [ hn, hp, hm ] = calculateh1( nu, mu, RE )
%calculateh1
% Calculates the scale factors for the Dipole Coordinate System
% Returns a 2-D matrix of scale factors with values at every
spatial
% location in the simulations at arbitrary phi.
alpha=(256/27)*(mu'.^2)*(nu.^-4);
beta=(1+(1+alpha).^0.5).^(2/3);
gamma=(alpha).^(1/3);
k=0.5*((beta.^2+beta.*gamma+gamma.^2)./(beta)).^1.5;
r=- (4*k./((1+k).*(1+(2*k-1).^0.5)))*(diag(RE*(nu.^-1)));
costheta=(RE^-2)*diag(mu)*(r.^2);
sintheta=(1-costheta.^2).^0.5;

hn=((r.^2)./(RE*(sintheta).*(1+3*(costheta).^2).^0.5))';
hm=((r.^3)./((RE^2)*(1+3*(costheta).^2).^0.5))';
hp=(r.*sintheta)';
```

#### 6.1.4. plot\_mer.m

```
function [ ] =
plot_mer(E,r,sintheta,costheta,psource,RE,PML,Title,Xaxis,Yaxis)
%Plot the Quantity in Meridional Plane
%Plots the distribution of Quantity E in the Meridional Plane of the
Dipole
%Coordinate system

figure3=figure;
axes3 = axes('Parent',figure3);
pcolor(squeeze(r(:,:,psource)).*squeeze(sintheta(:,:,psource))./RE,sq
ueeze(r(:,:,psource)).*squeeze(costheta(:,:,psource))./RE,(E(:,:,psou
rce))), 'Parent',axes3);colorbar;
shading('interp');
view([0 90]);
title(Title);
xlabel(Xaxis); ylabel(Yaxis);
colorbar;
% caxis([-6.96e-10 6.96e-10]);
hold on;
plot (cos(0:0.1:2*pi+0.1),sin(0:0.1:2*pi+0.1),'white');
hold on;
plot (squeeze(r(:,PML,psource)).*squeeze(sintheta(:,PML,psource))./RE,
squeeze(r(:,PML,psource)).*squeeze(costheta(:,PML,psource))./RE,'whit
e');
hold off;

end
```

#### 6.1.5. plot\_equ.m

```
function [ ] = plot_equ(E,r,sinphi,cosphi,m1,RE,Title,Xaxis,Yaxis)
%Plot the Quantity in Meridional Plane
%Plots the distribution of Quantity E in the Meridional Plane of the
Dipole
%Coordinate system

figure3=figure;
axes3 = axes('Parent',figure3);
pcolor(squeeze(r(m1,,:)).*(cosphi)./RE,squeeze(r(m1,,:)).*(sinphi).
/RE,(squeeze(E(:,m1,:))), 'Parent',axes3);colorbar;
shading('interp');
view([0 90]);
title(Title);
xlabel(Xaxis); ylabel(Yaxis);
colorbar;
hold on;
plot (cos(0:0.1:2*pi+0.1), sin(0:0.1:2*pi+0.1),'white');
hold off;

end
```

### 6.1.6. plot\_fft\_a.m

```
function [ ] = plot_fft_a( )
%PLOT_FFT_A Plots the Dispersion Diagram using values from
calculate_fft.mat

% Loading variables
load('calculate_fft.mat', 'NFFT', 'SFFT', 'deltat', 'time_tot',
'dmus', 'mu', 'nu', 'mus', 'msource', 'nsource', 'frequency', 'Fw');
load('calculate_fft.mat', 'NFFTa', 'deltat_a', 'time_tot_a', 'c2');

fmax=frequency+Fw/2;
Lsource=-1/nu(nsource);
musource=mu(msource);
% Creating the axes points to display in the Dispersion diagram
f=(1/(deltat_a))*linspace(-0.5,0.5,NFFTa);
K=(1/dmus)*linspace(-0.5,0.5,SFFT);
f1=1/(deltat_a)/2;
nmax=round(fmax*(NFFTa/2)/f1);
% Plotting the dispersion diagram
figure;
surf(K(1:SFFT),f(NFFTa/2-nmax:NFFTa/2+nmax),(log(c2(NFFTa/2-
nmax:NFFTa/2+nmax,1:SFFT))));
colorbar;shading interp;view ([0 90]);
ylim([0 fmax]);
xlim([min(K) max(K)]);
title(['|Space-TimeFFT (B_\phi(x,t))| [L_s=',num2str(Lsource,3),';
\mu_s=',num2str(musource,3),'; t_f =
',num2str(time_tot_a*deltat_a*10^3,4), ' ms; x_f =
',num2str(max(mus)*10^-3,6), ' km; f_c = ',num2str(frequency,4), ' Hz;
f_F_W_H_M = ',num2str(Fw,4), ' Hz]'],'FontSize',13);
xlabel('Wavenumber \kappa (m^-1)','FontSize',11); ylabel('Frequency
\omega (Hz)','FontSize',10);

end
```

## 6.2. Extracting plasma density from GCPM Ver 2.4

The following FORTRAN (gfortran compiler) code had to be used to extract data from GCPM ver 2.4. The functions required for the FORTRAN code can be downloaded from the ref: [18].

### 6.2.1. Input file: input.txt

```
2002197                #itime
6      30      0        #ihr,imin,isec
4.0                    #akp
6371200                #RE in meters
-0.01  0.001  0.25     #dn,dm,dp (where dp is in units of 2*pi)
0.8     10            #Li,Lf
1      -1              #Sm,Sm1
0      1                #Sp,Sp1 in units of 2*pi
```

### 6.2.2. main1.for

```
c      Program: main1.for
c      This program outputs the plasma density in the
c      plasmasphere for an entire nu-mu plane.
c      Input: ../input/input.txt
c      Output: ../output/e_den.dat
c
c      Author: Nithin Sivadas
c      Date   : 26th Jan 2013
c
c      Program main
c
c      real, parameter :: pi = 4*atan(1.0)
c      real*4 outn(4)
c      real*4 alatr,amlt,akp,RE
c      real*4 dn,dm,dp,Li,Lf,Sn,Sn1,Sm,Sm1,Sp1,Sp
c      integer*4 itime(2),ihr,imin,isec,i,j,q,Nn,Nm,Np
c      real, dimension(5000) :: mu,nu,phi
c      real, dimension(5000,5000) :: r,alpha,beta,gamm,k,e_den
c      real, dimension(5000,5000) :: costheta,theta
c
c      Input parameters from Text File Input.txt
c
c      open(unit=1,file='../input/input.txt')
c      read(1,*) itime(1)
```

```

read(1,*) ihr, imin, isec
read(1,*) akp
read(1,*) RE
read(1,*) dn, dm, dp
read(1,*) Li, Lf
read(1,*) Sm, Sm1
read(1,*) Sp, Sp1
close(unit=1)

```

```

itime(2)=(ihr*3600 + imin*60 + isec) * 1000
dp =dp*2*pi

```

```

Sn=-1/Li
Sn1=-1/Lf

```

```

Sp=Sp*2*pi
Sp1=Sp1*2*pi

```

```

Nn=NINT((Sn-Sn1)/dn) + 1
Nm=NINT((Sm-Sm1)/dm) + 1
Np=NINT((Sp1-Sp)/dp) + 1

```

```

mu(1)=Sm1
nu(1)=Sn1
phi(1)=Sp

```

```

amlt=16.0

```

```

c   Printing the acquired inputs on screen
print *, 'itime(1) : ',itime(1)
print *, 'itime(2) : ',itime(2)
print *, 'ihr: ',ihr,' imin: ',imin,' isec: ',isec
print *, 'akp: ',akp
print *, 'RE: ', RE
print *, 'dn: ',dn,' dm: ',dm,' dp: ',dp
print *, 'Li: ',Li,' Lf: ',Lf
print *, 'Sm: ',Sm,' Sm1: ',Sm1
print *, 'Sp: ',Sp,' Sp1: ',Sp1

```

```

c   Creating the required arrays
do i=2,Nm
    mu(i) = mu(i-1)+dm

```

```

end do
do j=2,Nn
    nu(j) = nu(j-1)+dn
end do
do q=2,Np
    phi(q) = phi(q-1)+dp
end do

c    Converting from Dipole to Spherical Coordinates
!$OMP DO
do i=1,Nn
alpha(:,i)=(256.0/27.0)*(mu**2.0)/(nu(i)**4.0)
beta(:,i)=(1+(1+alpha(:,i))**0.5)**(2.0/3.0)
gamm(:,i)=(alpha(:,i))**(1.0/3.0)
k(:,i)=((beta(:,i)**2+beta(:,i)*gamm(:,i)+gamm(:,i)**2)**1.5)
k(:,i)=0.5*k(:,i)/((beta(:,i))**1.5)
r(:,i)=-(4*k(:,i)/((1+k(:,i))*(1+(2*k(:,i)-1)**0.5)))
r(:,i)=r(:,i)*(RE/(nu(i)))
costheta(:,i)=((1/RE**2.0)*mu*(r(:,i)**2.0))
theta(:,i)=acos(costheta(:,i))-(pi/2.0)
end do
!$OMP END DO
open(unit=1,file='../output/e_den.dat')

c    Extracting Plasma density values from GCPM v2.4
print *,'Calculation Started'
!$OMP DO
do i=1,Nm
    do j=1,Nn
        call gcpm_v24(itime,r(i,j)/RE,amlt,theta(i,j),akp,outn)
        e_den(i,j)=outn(1)
    end do
    write(1,*) e_den(i,1:Nn)
end do
!$OMP END DO
close(unit=1)

    print *,'Output stored in ../output/'
print *,'Matrix Dimensions are Nm: ',Nm,' Nn: ',Nn
print *,'*****Run Successful*****'

end program main

```

### 6.3. 3-D Particle Trajectory Solver

This simulation module consists of the following MATLAB script files and functions:

1. `lineartrap.m` : This is the main script file, that inputs the required variables from 3-D FDTD simulation results to generate the Alfvén wave noise, and then solve for the particle's trajectory in the geo-magnetic field with Alfvén wave noise superposed on it. The programs input is 'calculate\_fft.mat' and 'V2.mat' generated from the 3-D FDTD simulations. The output trajectory of the particles and equatorial pitch angle distributions are stored in 'results.mat'.
2. `solve1.m()` : This is a function that implements the 4-th order runge-kutta algorithm to solve for the position and velocity of the particle using only the Newton-Lorentz equation of motion.
3. `cart2dip()` : This is a function that converts Cartesian coordinates to Dipole coordinates.
4. `equatorial_pitch()`: This function calculates the Equatorial pitch angles of the particle whenever it crosses the equatorial plane. It returns the equatorial pitch angle, and the time at which it crossed the equatorial plane.
5. `velocity()`: This function returns the parallel, perpendicular velocities and the pitch angle of the particle at every sample point in space.
6. `Bfield_1()`: This function defines the required dipole magnetic field without incorporating any wave perturbations.

This matlab script was made and run in MATLABr2012a in the VIRGO supercluster at IIT Madras.

### 6.3.1. lineartrap.m

```
% Simple Linear Magnetic Trap for a Single Particle

clc;
clear all;

tic;

% Defining Key Constants/ Parameters
e=1.66e-19;           % Electronic charge in Coulombs
m=1.625e-27;         % Mass of a proton in Kg
c=3e+8;              % Speed of light
wave_power=6*10^-9; % Defining the RMS power of the alfven wave
RE=6.3712e+06;       % Mean radius of Earth

% Definig paramters
KE=1.0000000;        % Energy of the particle in MeV
Tot_time=2;          % Time of running the simulation (in seconds)

% Defining Simulation Space

Ls=1.4286; % L-shell of origin of the particles

samples=20000; % Number of time samples from start of the simulation
to the end

% Calculating required variables
v=c*(1-(KE*(1.602*10^-13)*(m*c^2)^-1+1)^-2)^0.5; % Relativistic
Velocity
% Starting point of the particles in terms of Dipole Coordinates
nsource=-1/Ls;
msource=0;
psource=0;

% Interface variables from 3D-FDTD Simulations
load('calculate_fft.mat','time_tot_a','deltat_a','mu','c2','SFFT','NF
FTa');
load('V2.mat');

% Variables required for calculation
dm=mu(2)-mu(1);
mu2=-1:dm:1;
l1=size(mu2);
SFFT2=l1(2);
a1=round((mu(1)-mu2(1))/dm+1);
b1=round((mu(SFFT)-mu2(1))/dm+1);

%% Calculating the Noise Signal
fmax=1000;
f1=1/(deltat_a)/2;
nmax=round(fmax*(NFFTa/2)/f1);
p=size(NFFTa/2-nmax+1:NFFTa/2+nmax);
SFFT1=SFFT;

    for j=1:1:SFFT1
```

```

        c2(NFFTa/2-nmax+1:NFFTa/2+nmax,j)=c2(NFFTa/2-
nmax+1:NFFTa/2+nmax,j).*tukeywin(p(2)); %tukey window to avoid any
abdrupt jumps in the f-k space
        end;

Bp2=zeros(time_tot_a,SFFT2);
Bp3=zeros(time_tot_a,SFFT2);
V3=zeros(1,SFFT2);
Bp_rms=zeros(SFFT2,1);
crand=zeros(NFFTa,SFFT1);
RandSignal=zeros(NFFTa,SFFT1);

alpha1=60; % Pitch Angle of the Particle (in degrees)
for var=1:1:2

% Alfven-wave Noise
var
prand=-pi + 2*(pi).*rand(p(2),SFFT1); %Randomized phase
crand(NFFTa/2-nmax+1:NFFTa/2+nmax,1:1:SFFT1)=(abs(c2(NFFTa/2-
nmax+1:NFFTa/2+nmax,1:1:SFFT1))).*exp(1i*prand);
RandSignal(1:1:NFFTa,1:1:SFFT1)=ifft2(fftshift(crand)*SFFT1*NFFTa,NFF
Ta,SFFT1,'nonsymmetric');
Bp=real(RandSignal);

%% Modifying the Magnetic field noise for the ODE solver
Bp2(:,a1:1:b1)=Bp(:,1:1:SFFT);
V3(1,a1:1:b1)=V2(1,1:1:SFFT);
time=(1:1:time_tot_a)*deltat_a-deltat_a;
for i=1:1:SFFT2
    Bp_rms(i,1)=(sum(Bp2(:,i).^2).*deltat_a)/max(time);
end;
Bp_power=Bp_rms/(2*4*pi*10^-7);
Bp_power_set=wave_power*ones(SFFT2,1);
Bp_rms_set=Bp_power_set*(2*4*pi*10^-7);

for i=1:1:SFFT2
    Bp3(:,i)=(Bp2(:,i)./(Bp_rms(i)).^0.5)*(Bp_rms_set(i)).^0.5;
end;

%% Generating E-field noise
for i=1:1:NFFTa
    En3(i,:)=Bp3(i,:).*V3.^0.5;
end;
alpha=alpha1*pi/180;% Pitch angle in radians
x0=[Ls*RE 0 0];
v0=[0 v*sin(alpha) v*cos(alpha)];

% Solving the differential equation (Newrton-Lorentz force equation)
[T,W]=solvel(time,Tot_time,samples,x0,v0,e,m,c,RE,Bp3,mu2,dm,En3);
a=size(W); % The number of samples of the path of the particle

%% Estimating the Equatorial Pitch Angle Distribution
[eq_pitch,time_pitch] = equatorial_pitch( W,samples,Tot_time );
eq_pitch_angle(var)=eq_pitch(1);
alpha_0(var)=alpha1;
end;

toc;
save('results.mat');

```

### 6.3.2. solve1.m

```
function [T,W] =
solve1(time,Tot_time,samples,x0,v0,e,m,c,RE,Bp,mu,dm,En)
%SOLVE1 Implements the 4th Order Runge-Kutta Algorithm
% to solve for the position and velocity of the particle using only
% the Newton-Lorentz equation of motion.
options=odeset('RelTol',1e-6,'AbsTol',[1e-6 1e-6 1e-6 1e-6 1e-6 1e-
6]);
tspan=linspace(0,Tot_time,samples);
[T, W]=ode45(@lorentzd,tspan, [x0(1) x0(2) x0(3) v0(1) v0(2)
v0(3)]',options);

function dw = lorentzd(t,w)
% Lorentzd is a function that represents the first order differential
% equation of particle motion using the lorentz force equation. It
% requires the position and velocity of the particle at a particular
% timestep t. It returns the derivatives of position and velocity at
% that time instant.

% The first order differential equation that represents the Lorentz
% force equations

dw=zeros(6,1);
period=floor(t/max(time));
t1=t-period*max(time);

% Converting particle coordinates from cartesian to Dipole
Coordinates
[nu1, mu1, phi1]=cart2dip(w(1),w(2),w(3),RE);

% Extracting the E and B field noise value at the position of the
particle
A=round((-mu(1)+mu1)/dm)-2:1:round((-mu(1)+mu1)/dm)+2;
if (isnan(mu1)~=1)
B_p_temp(1,1:1:5)=interp1(time,Bp(:,round(A)),t1);
B_p_noise=interp1(mu(round(A)),B_p_temp(1,1:1:5),mu1);
E_n_temp(1,1:1:5)=interp1(time,En(:,round(A)),t1);
E_n_noise=interp1(mu(round(A)),E_n_temp(1,1:1:5),mu1);
else
B_p_noise=0;
E_n_noise=0;
end;

% Converting the particle coordinates from cartesian to spherical
[phi,theta,r]=cart2sph(w(1),w(2),w(3));

% Converting the E and B field vectors from dipole to cartesian
coordinates
B_x_noise=-sin(phi).*B_p_noise;
B_y_noise=+cos(phi).*B_p_noise;
d1=(1+3*cos(theta).^2).^0.5;
d2=(1-3*cos(theta).^2)/d1;
E(1)=d2*cos(phi)*E_n_noise;
E(2)=d2*sin(phi)*E_n_noise;
E(3)=E_n_noise*1.5*sin(2*theta)./d1;
B0=3.07*10^-5;
RE=6.3712e+06;
r=(w(1).^2+w(2).^2+w(3).^2).^0.5;
A=-(B0*RE^3)/r^5;
```

```

B(1)=A*3*w(1)*w(3)-sin(phi).*B_p_noise;
B(2)=A*3*w(2)*w(3)+cos(phi).*B_p_noise;
B(3)=A*(2*w(3)^2-w(1)^2-w(2)^2);
gamma=(1-((w(4).^2+w(5).^2+w(6).^2)/c^2)^-0.5;

dw(1)=w(4); %Vnu Xnu
dw(2)=w(5); %Vmu Xmu
dw(3)=w(6); %Vphi Xphi

% Acceleration (increment in velocity)
dw(4)=(e/(gamma*m))*(E(1)+(B(3)*w(5)-B(2)*w(6)));
dw(5)=(e/(gamma*m))*(E(2)-(B(3)*w(4)-B(1)*w(6)));
dw(6)=(e/(gamma*m))*(E(3)+(B(2)*w(4)-B(1)*w(5)));
end

end

```

### 6.3.3. cart2dip.m

```

function [ nu,mu,phi ] = cart2dip( X,Y,Z,RE)
%cart2dip Function that converts from cartesian to Dipole Coordinates
[phi,theta,r]=cart2sph(X,Y,Z);
theta=theta-pi/2;
mu=(cos(theta)).*(RE./r).^2;
nu=- (RE./r).*(sin(theta)).^2;
end

```

### 6.3.4. equatorial\_pitch.m

```

function [ eq_pitch,time_pitch ] = equatorial_pitch(
W,samples,Tot_time )
%equatorial_pitch This function calculates the Equatorial pitch
angles
% of the particle whenever it crosses the equatorial plane.
dt=Tot_time/samples;
[V_para, V_perp, pitch_angle] = velocity( W,samples );
k=1;
eq_pitch=0;
time_pitch=0;
for i=1:1:samples-1
    if(W(i,3)*W(i+1,3)<0)
        equatorial_pitch(k,1:1:11)=pitch_angle(i-5:1:i+5);
        time_sample(k,1:1:11)=(i-5:1:i+5)*dt;
        z_coord(k,1:1:11)=W(i-5:1:i+5,3)';
    end
    eq_pitch(k)=interp1(z_coord(k,:),equatorial_pitch(k,:),0,'spline');
    time_pitch(k)=interp1(z_coord(k,:),time_sample(k,:),0,'spline');
    k=k+1;
end;
end;

end

```

### 6.3.5. velocity.m

```
function [ V_para, V_perp, pitch_angle ] = velocity( W,samples )
%VELOCITY returns the parallel, perpendicular velocities and the
pitch
%angle of the particle at every sample point in space.

for i=1:1:samples
    B(:,i) = Bfield_1([W(i,1), W(i,2), W(i,3)]);
end;

% Velocity vector along the path
V(:,1:samples)=W(1:samples,4:6)';

% Magnitude of velocity along the path
V_mag=(V(1,:).^2+V(2,:).^2+V(3,:).^2).^0.5;

% Magnetic field intensity along the path
B_mag=(B(1,:).^2+B(2,:).^2+B(3,:).^2).^0.5;

% Unit vector along the magnetic field
B_norm(1,:)=B(1,:)./B_mag;
B_norm(2,:)=B(2,:)./B_mag;
B_norm(3,:)=B(3,:)./B_mag;

%% Magnitude of Parallel and Perpendicular Velocity to the Magnetic
field line
V_para_temp=V.*B_norm;

V_para=V_para_temp(1,:)+V_para_temp(2,:)+V_para_temp(3,:); % Parallel
velocity
V_perp=(V_mag.^2-V_para.^2).^0.5; % Perpendicular Velocity
pitch_angle=(atan(V_perp./V_para))*180/pi;

end
```

### 6.3.6. Bfield\_1.m

```
function B = Bfield(w)
%Bfield defines the required dipole magnetic field without
incorporating
% any wave perturbations

% Parameters for calculating Earth's dipole magnetic field
B0=3.07*10^-5;
RE=6.3712e+06;
r=(w(1).^2+w(2).^2+w(3).^2).^0.5;
A=-(B0*RE^3)/r^5;

% Magnetic field values in X,Y and Z axis
B(1)=A*3*w(1)*w(3);
B(2)=A*3*w(2)*w(3);
B(3)=A*(2*w(3)^2-w(1)^2-w(2)^2);

end
```

## **APPENDIX II: Conference Poster**

A poster on this research work will be presented at the 2013 Workshop on ‘**Coupling, Energetics and Dynamics of Atmospheric Regions (CEDAR)**’ to be held at **Boulder, Colorado, USA (22 – 28 June, 2013)**. The conference is organized by the University Corporation for Atmospheric Research.

The details of the conference poster are as follows:

**Abstract Title: FDTD Modelling of Low-frequency Shear-Alfven-wave Propagation and its Interaction with Trapped Charge Particles in the Magnetosphere**

**Abstract:** This study presents test particle analysis of the scattering of high energy particles by shear Alfven noise in the Van-Allen radiation belts. The Alfven noise was generated by carrying out a Finite Difference Time Domain (FDTD) simulation of shear-Alfven-wave modes, using realistic values of plasma parameters and perfectly-reflecting ionosphere boundary conditions. The purpose of the study is to understand the statistics of high energy particle scattering into the near earth region of the ionosphere.

**Authors:** Nithin Sivadas, Dr. H. Ramachandran, Dr. T. M. Muruganandam

Please see the next page for a copy of the invitation letter.



UNIVERSITY CORPORATION FOR ATMOSPHERIC RESEARCH

NATIONAL CENTER FOR ATMOSPHERIC RESEARCH | UCAR OFFICE OF PROGRAMS

May 13, 2013

Nithin Sivadas  
Indian Institute of Technology Madras  
Te-Net Office  
Department of Electrical Engineering  
Chennai, TN, PIN-600036  
India

Dear Nithin Sivadas,

It is my pleasure to invite you to attend the 2013 CEDAR Workshop to be held at the Millennium Hotel in Boulder, CO, from June 22-June 28, 2013. UCAR will waive your graduate student registration fee and provide your per diem and lodging in the shared student housing located at the Millennium Hotel.

We look forward to your attending this workshop and presenting your posters titled "FDTD Modeling of Low-frequency Shear-Alfven-wave Propagation and its Interaction with Trapped Charge Particles in the Magnetosphere" and "Space based Proton Electron Detector (SPEED) to Measure Fluctuations in the Energy Spectra of Protons and Electrons in the Upper Ionosphere". This is an excellent opportunity to meet and talk with other colleagues in your research community.

Sincerely,

Kendra Greb  
Organizer  
2013 CEDAR Workshop  
<http://cedarweb.hao.ucar.edu>